THE ASTROPHYSICAL JOURNAL, 321:622–644, 1987 October 15

THE DYNAMICS OF SMALL GROUPS OF GALAXIES. I. VIRIALIZED GROUPS

GARY A. MAMON
Princeton University Observatory and New York University
Received 1986 October 27; accepted 1987 March 12

ABSTRACT

A numerical code is developed to follow the dynamical evolution of groups of galaxies, starting from virial equilibrium. The code assigns a single particle to each galaxy and to a diffuse intergalactic background, both with appropriately softened potentials, and explicitly incorporates many of the physical processes occurring in groups, such as collisional stripping, tidal stripping from the background mean field, dynamical friction on the background, mergers, and orbital braking.

Groups of eight galaxies with surface densities similar to Hickson's compact groups are unstable against rapid galaxy merging and fail to meet Hickson's compact group selection criteria (by lack of membership) after typically 6 or 30 half-mass crossing times [1/30 or $(1/8)t_{\rm Hubble}$], depending on whether or not the dark matter is mainly in galactic halos or in a common intergalactic background. Statistical fluctuations cause two-thirds of the groups to evolve in one-half to twice the median rate, and no dense groups of eight galaxies still appear compact (in Hickson's sense) after $\frac{1}{2}t_{\rm Hubble}$. These "instability" times are insensitive to the uncertainties of the physics used in the code, but are increased with larger group membership, and larger group mass-luminosity ratios.

Loose groups of eight galaxies typically witness two to four mergers with $t_{\rm Hubble}$. Compact subgroups (as defined by Hickson) are seen in projection in 3%–35% of the loose groups. In loose groups of galaxies with massive halos, the compact subsystems are almost all chance alignments of galaxies, whereas in loose groups of galaxies without massive halos, half are chance alignments and the remainder are part of three-dimensional cores, a small fraction of which are bound.

The cumulative luminosity function of dense groups shows statistical signs of mergers at its bright end halfway toward instability, while in loose groups these signs appear after $\frac{1}{2}t_{\rm Hubble}$. Luminosity segregation occurs even faster. Tidal truncation is evident only in groups of galaxies without massive halos.

Subject headings: galaxies: clustering — galaxies: evolution — galaxies: structure — numerical methods

I. INTRODUCTION

Although most galaxies are located within small groups (e.g., van den Bergh 1962; de Vaucouleurs 1975; Bahcall 1979), the dynamical evolution in these settings has not generated much interest among astrophysicists, who have preferred the study of the more glamorous rich clusters. Perhaps workers have been put off by the erratic behavior of galaxies in small groups (Aarseth and Saslaw 1972; Giuricin *et al.* 1984). Recently however, several "self-consistent" numerical codes have been developed with galaxies made up of a collection of stars (Carnevali, Cavaliere, and Santangelo 1981; Ishizawa *et al.* 1983; Cavaliere *et al.* 1983; Barnes 1985), thus allowing for the first realistic studies of dense groups of galaxies.

In studying groups of galaxies, one is attempting to answer fundamental questions on their dynamical nature: Are small groups bound dynamical systems? Have the majority of them reached equilibrium conditions well described by hydrodynamic equations and the virial theorem? What constitutes the dark matter whose presence is inferred from such equilibrium treatments of groups? These questions are complicated by the fact that groups of galaxies occur in a wide range of densities, from our Local Group, which must not have virialized yet but is instead just turning around from its initial Hubble expansion (Gunn 1974), to the compact groups, some of which appear so tightly packed in projection that their galaxies overlap (e.g., Hickson 1982). Moreover, group densities are poorly known because of the strong sensitivity of present-day mass estimators to interlopers, and this prevents the evaluation of group evolution time scales.

It was initially thought that small groups of galaxies of roughly equal mass would be unstable to *evaporation* in a few group crossing times (Ambartsumian 1961). Later, Toomre and Toomre (1972) showed that the inelastic nature of galaxy encounters leads pairs of sufficiently slowly colliding galaxies to merge into a single entity. Small groups have low enough velocity dispersions for a significant fraction of interpenetrating encounters of galaxies to lead to merging. A "cannibal" galaxy develops and grows on a time scale of a few crossing times, and its increased cross section further enhances the rate of accretion of smaller galaxies, thus leading to a *merging* instability (Ostriker and Hausman 1977).

Whether or not an encounter is slow enough for merging to occur, it produces tides in the individual galaxies that are efficient in removing matter from the galaxies, some of which settles into a diffuse intergalactic medium. This background of dark matter and tidally stripped matter should in turn play an important role in the evolution of the group, since tides produced by its mean field limit the sizes of galaxies (e.g., Merritt 1984) and since dynamical friction is responsible for extracting orbital energy from the galaxies (Chandrasekhar 1943). These two processes have opposite effects on the stability of the group. Dynamical friction causes the galaxies to decay toward the center of the diffuse background (Tremaine, Ostriker, and Spitzer 1975), where they are more likely to have close encounters, and merge, while mean-field tidal limitation reduces the merger rate, both directly by reducing the merger cross sections and indirectly by reducing the rate of orbital decay.

This study was begun with the idea that some dense aggregates of galaxies could survive over relatively long periods of time, if the merging instability is tempered in the three following ways. First, two-body relaxation may be effective in establishing a hierarchy of orbits which prevent the galaxies from closely interacting at each passage. By choosing equal galaxy masses, Carnevali, Cavaliere, and Santangelo (1981) and Ishizawa *et al.* (1983) effectively prevented this from occurring in their numerical simulations; hence their short merging times. Second, the rates of direct merging and of orbital decay are reduced if tidal processes are efficient in groups. Finally, while the time scale for the merging instability should be a small fraction of the Hubble time *on the average*, it need not be *for all groups of galaxies*, and small-number statistics may push the time scale for $N - 3$ galaxies to merge (thus reducing the group to a triplet) to a value comparable to the Hubble time, for a small but nonnegligible number of cases.

The nonlinear evolution predicted by the stochastic nature of the dynamics of small systems and by the interaction of different physical processes makes analytical solutions inadequate, and therefore an N-body treatment is required. For a decent statistical coverage, it is clear that the self-consistent simulations of the Carnevali, Cavaliere, and Santangelo (1981) type are too costly, and a more elaborate, faster, but less self-consistent gravitational N-body code is developed, in which galaxies and a diffuse background are all treated as single particles. The lack of self-consistency of the method described in § II requires the explicit inclusion of the physical processes operating in groups of galaxies, and this is presented in § III. The initial particle parameters are set forth in § IV, while § V is concerned with the numerical features and tests. Results are presented in § VI and discussed in § VII. This article concerns itself with the evolution of groups from virialized initial conditions. A following article (Mamon 1987*b*) will be devoted to the study of groups from their initial Hubble expansion.

II. METHOD

The basic scheme is a gravitational N-body code, in which galaxies and a diffuse background are all treated as single particles, with external parameters such as mass, luminosity, internal energy, and tidal radius, but also with internal structure: the particles are assigned mass and luminosity profiles, from which the remaining internal parameters, such as core radius and central density, are easily obtained. This scheme explicitly incorporates physical processes such as dynamical friction of galaxies against the background, galaxy mergers, collisional stripping, tidal limitation of galaxies by the mean field of the background, and orbital braking in inelastic encounters. For a set of physical parameters, 20 or 50 groups that differ only by the Monte Carlo initialization of galaxy positions, velocities, and masses are evolved for a Hubble time. This scheme requires only $N + 1$ particles, where N is the number of galaxies in the group. The computation time for a single run is thus very short, which allows $\sim 10^3$ runs to be performed. With this method, the relative importance of a given physical mechanism can be assessed by simply turning it off.

The particles representing galaxies are modeled for simplicity as spherically symmetric mass distributions, with density

$$\rho(r) = \frac{\rho(0)}{[(r/r_c)^2 + 1]^{n/2}}, \tag{1}$$

where r_c is the galaxy core radius, and with $n = 2$ for "halo" models (representing spiral or elliptical galaxies with massive halos), and $n = 3$ for "modified Hubble" models (representing ellipticals with constant M/L). The mass distributions in equation (1) are sharply truncated at a tidal radius $r = r_t$. Note that the truncated version of the modified Hubble model approximates well an $r^{1/4}$ law in projection (Mamon 1985, hereafter M85, § IV*a*). The particle representing the intergalactic background is also assigned a spherically symmetric modified Hubble mass distribution, truncated at 15 core radii (as used by Schneider and Gunn 1983).

III. BASIC PHYSICS

a) Equations of Motion

The total force on each galaxy is the sum of three terms: the gravitational forces arising from each of the other galaxies, the gravitational force from the background potential gradient, and the dynamical friction force that the background exerts on the galaxies. The force on the background is taken as the exact opposite of the sum of the forces felt by the galaxies, giving a zero net force on the group.

i) *Potential Energy of Interaction of Two Overlapping Spheres*

Since the numerical scheme developed in this work attributes only one single particle to each galaxy, whereas galaxies are extended systems, often overlapping in dense groups, it is necessary to use softer force laws than the usual Newtonian one. For energy to be conserved, the force between two galaxies must be derived from a potential energy of interaction, which is expressed as the potential energy of interaction of the two galaxies placed concentrically, normalized to the real separation with a dimensionless extrapolation function (this avoids recomputing a double integral at every time step):

$$V_{\rm int}(R) = V_{\rm int}(0)\tilde{V}(R/R_0) . \tag{2}$$

For the galaxy and background models described in § II, the potential energy of interaction of the two galaxies placed concentrically, $V_{\rm int}(0)$, is evaluated by cubic spline interpolation of pretabulated computed values (M85, Appendix B). The softening parameter in equation (2) is

$$R_0 = \frac{GM_1M_2}{V_{\rm int}(0)} , \tag{3}$$

and the extrapolation function is chosen as

$$\tilde{V}(Y) = (Y^2 + 1)^{-1/2} . \tag{4}$$

Equations (2), (3), and (4) yield the correct limits for V at $R = 0$ and $R \to \infty$, but not at $R = r_{t_1} + r_{t_2}$; they also produce the correct limit at $R = 0$ for dV/dR. The potential energy of interaction between a galaxy and the background is derived in exactly the same fashion. For the adopted galaxy and background mass distributions (§ II), the approximation of equations (2), (3), and (4) is found in most cases to be exact to roughly 20% accuracy for $R > R_0/2$ (M85, § II*a*[i]). With these mass distributions, R_0 is close to the rms half-mass radius of the galaxies: $R_0 \approx [(r_{h_1}^2 + r_{h_2}^2)/2]^{1/2}$ (M85, § II*a*[i]). Note that most authors in the field of large-scale N-body simulations have chosen different softening lengths from the ones above. Roos and Norman (1979) and Rose (1979) respectively took fixed softening lengths of 25 kpc and 55 kpc, which were much too large, even assuming that galaxies have r^{-2} halos. Aarseth and Saslaw (1972) and Cooper and Miller (1981) adopted a fixed softening length in terms of a closest neighbor distance. The softening lengths of Roos (1981) and Roos and Aarseth (1982), which were typically one-half of the tidal radius of the largest of the two galaxies, agree with the softening scale adopted here only if galaxies possess dark halos. On the other hand, Aarseth and Fall (1980) and Farouki and Shapiro (1982) selected softening lengths that both scale as the rms half-mass radius to within a few percent.

ii) *Dynamical Friction*

From the analysis of Chandrasekhar (1943), the force of dynamical friction, which the background exerts on a galaxy of radial coordinate R_α and velocity V_α in the background frame, is

$$\boldsymbol{F}_{\mathrm{df}_\alpha} = -\frac{4\pi G^2 M_\alpha^2 \rho_{\mathrm{bg}}(R_\alpha)[\mathrm{erf}\,(x_0) - x_0\,\mathrm{erf}'\,(x_0)]\ln\Lambda}{V_\alpha^3}\boldsymbol{V}_\alpha\,, \tag{5a}$$

$$x_0 = 2^{-1/2}\frac{V_\alpha}{\sigma_{\mathrm{bg}}(R_\alpha)}\,, \tag{5b}$$

where $\rho_{\mathrm{bg}}(R_\alpha)$ and $\sigma_{\mathrm{bg}}(R_\alpha)$ are the local background density and velocity dispersion, respectively. The term in brackets represents the fraction of particles whose velocity magnitude is below V_α for a Maxwellian velocity distribution. Note that the mass of the particle that constitutes the background (e.g., stars, brown dwarfs, neutrinos, axions) should be small in comparison with galaxy masses, and was neglected in equation (5).

The Coulomb logarithm in equation (5a) can be written

$$\ln\Lambda = \ln\left(\frac{p_{\mathrm{max}}}{p_{\mathrm{min}}}\right)\,, \tag{6}$$

where p_{max} and p_{min} are the maximum and minimum impact parameters for which collisions with background particles are effective in altering the orbits of the galaxies. Following Tremaine, Ostriker, and Spitzer (1975), the maximum impact parameter is chosen as

$$p_{\mathrm{max}} = \max\,(R_\alpha, R_c)\,, \tag{7}$$

where R_c is the background core radius. The minimum effective impact parameter for extended test particles of concentration parameter $x_t = r_t/r_c$ is taken from White's (1976) equation (6), which, for the two galaxy models adopted in this present work (eq. [1]), yields

$$\frac{p_{\mathrm{min}}}{r_t} = 0.589 x_t^{-0.044}\,, \tag{8a}$$

$$\frac{p_{\mathrm{min}}}{r_t} = 0.794 x_t^{-0.324}\,, \tag{8b}$$

for halo models and modified Hubble models, respectively, and hence $p_{\mathrm{min}} \approx r_h$ for both mass distributions (see M85, § II*a*[ii]). The Coulomb logarithms obtained from equations (6), (7), and (8) ranged from 1 to 5, which is in agreement with the choices of most workers in the field, except for Richstone and Malumuth (1983), who adopted $\ln\Lambda = 10$. Dynamical friction is turned off when $\Lambda < 1$.

b) Tidal Limitation by the Mean Background Field

It has long been assumed that the sizes of globular clusters are determined by the mean tidal field of the surrounding galaxy (King 1962). Similar arguments concerning the tidal limitation of galaxies by the mean field of the cluster have been presented by Peebles (1970) and Gunn (1977), and recently Merritt (1984) incorporated this mechanism in a cluster evolutionary scheme by assuming that the tidal effects are set from the collapse phase of the cluster.

A precise determination of the effects of background tides on the sizes of galaxies is a difficult problem because several approximations are inadequate. First, for two point masses in circular orbit, test particles will be constrained inside two *Roche* lobes, one surrounding each point mass, tangent at an intermediate (second Lagrangian) point. The boundaries of the Roche lobes are frozen in the corotating frame, and can be calculated exactly. However, the Roche radius is not applicable in the present situation of an extended galaxy moving on elongated orbits.

A second approximation often made is that the tide acts instantaneously on the galaxy. The tidal radius is then defined by setting to zero the acceleration of a test star lying along the symmetry axis, relative to the center of the galaxy, *in the rotating frame:*

$$\begin{aligned}\frac{d^2r}{dt^2} &= 0\\ &= -\phi_g'(r) - [\phi_{\mathrm{bg}}'(R+r) - \phi_{\mathrm{bg}}'(R)] + \Omega^2 r\,,\end{aligned} \tag{9}$$

where R and r are the distance of the galaxy to the center of the background and the galactocentric position of the test star, respectively, and Ω is the tangential angular velocity of the galaxy and background around their mutual center of mass, and where the Coriolis inertial forces due to the motions of the star in the rotating frame have been neglected. This formulation is due to King (1962), who solves equation (9) by expanding ϕ_{bg}' in a Taylor series around R, and finds that the tidal radius is a decreasing function of orbit eccentricity (at constant pericenter).

However, if the galaxy is on an elongated orbit, the tide will be of short duration and stars will not have time to reach escape velocity. The Roche problem is better understood as a tidal shock (e.g., Ostriker, Spitzer, and Chevalier 1972), and simple results can be obtained analytically with the impulse approximation, developed by Spitzer (1958), in which the motion of a test particle is assumed to be small, and where the perturber is assumed to move at constant velocity in a straight line about the test object. Spitzer's calculations relate to a point-mass perturber, and a test object that is small in comparison with the impact parameter, but can readily be generalized to the case of a diffuse perturber. In both cases, the impulse approximation produces stellar velocity increments $\Delta v \sim 1/V$, where V is the velocity of the perturber relative to the stellar system (see eq. [8] in Spitzer 1958, and eqs. [A1] and [A2] of this paper). Thus, *for orbits of given pericenter, the net effects of tides and the tidal radii of stellar systems are respectively decreasing and increasing functions of orbit eccentricity, contrary to what is inferred from King's (1962) analysis.* The limiting radii of galaxies on elongated orbits inside groups or clusters should thus be larger than the corresponding radii of galaxies on circular orbits. Note that preliminary numerical results by Merritt and White (1987) suggest that at a given pericenter, tides may be strongest at some intermediate orbit elongation.

In Figure 1 the tidal radii calculated from the instantaneous tidal approximation (*open symbols*), solving equation (9), and from the impulse approximation (*filled symbols*), solving equa-

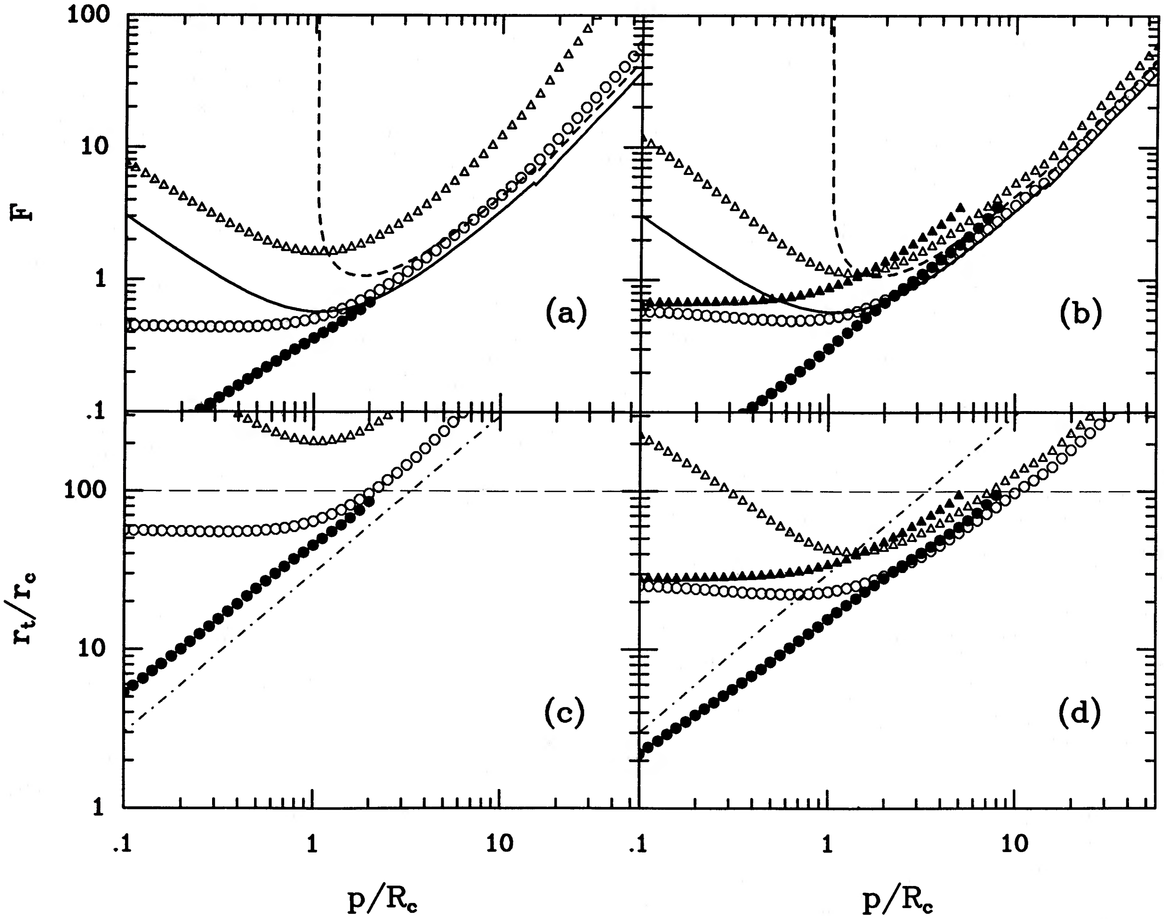

FIG. 1.—Limiting radii of halo (*a*, *c*) galaxies and modified Hubble galaxies (*b*, *d*), both with $R_c/r_c = 30$ and $(\rho_p R_c^2)/(\rho_g r_c^2) = 1$, as a function of impact parameter for a modified Hubble perturber with $X_t = 15$, expressed in terms of F (defined in eq. [10]) (*a*, *b*) or in terms of the concentration parameter x_t (*c*, *d*). *Solid curve*: Instantaneous tidal radius for circular galactic orbits obtained by Taylor series expansion of eq. (9). *Dashed curve*: Instantaneous tidal radius for radial galactic orbits obtained by Taylor series expansion of eq. (9). The break in these curves at $p/R_c = 15$ is an artifact of the sharp truncation of the perturber. *Open circles*: Instantaneous tidal radius (eq. [9]) for circular galactic orbits. *Open triangles*: Instantaneous tidal radius for radial galactic orbits. *Filled circles*: Impulse approximation radius (eq. [A5]) for circular galactic orbits. *Filled triangles*: Impulse approximation radius for "parabolic" (zero-energy) galactic orbits. *Dash-dot line*: Radius for which the galaxy just overlaps the center of the perturber at closest approach. *Thin dashed line*: Initial galaxy radius.

tion (A5), are plotted as a function of distance to the center of the cluster. The instantaneous tidal radii are computed at each radius for circular orbits (*circles*) and radial orbits (*triangles*), while the tidal radii derived from the impulse approximation are computed at the orbit pericenter for circular orbits (*circles*) and "parabolic" zero-energy orbits (*triangles*). The upper plots refer to the parameter F, introduced by Merritt (1984), defined by

$$r_t/R_c = 2^{1/2} v_c(r_t) \sigma_p^{-1} F(R/R_c) , \qquad (10)$$

where $v_c(r)$ and σ_p are the circular velocity at galactocentric radius r and the perturber central one-dimensional velocity dispersion, respectively, and R_c is the core radius of the perturber. For a modified Hubble diffuse perturber, F can be written as

$$F = 0.41 \frac{\omega_p(0)}{\omega_g(r_t)} , \qquad (11)$$

where $\omega_g(r)$ and $\omega_p(p)$ refer to the galaxy angular circular velocity and the perturber angular velocity at pericenter, respectively. The lower plots in Figure 1 give the resultant galaxy concentration parameter. For reference, the solutions to equation (9) obtained by Taylor series expansion of the tidal field are shown for circular (*solid curve*) and radial (*dashed curve*) orbits (the first curve is analogous to Merritt's Fig. 1). This figure shows the usefulness of F: it is very insensitive to the scaling of the galaxy relative to the perturber but depends almost uniquely on the impact parameter and the orbital eccentricity of the orbit of the galaxy about the perturber. This has been checked by varying R_c/r_c, and $(\rho_p R_c^2)/(\rho_g r_c^2)$, around their respective values of 30 and 1, used in Figure 1 (M85, § II*b*), where ρ_p and ρ_g are respectively the perturber and galaxy central densities.

Note that the tidal radii obtained with the impulse approximation depend on the initial value of x_t, since the dimensionless squared velocity dispersion $\tilde{\sigma}^2$ and potential $\tilde{\phi}$ appearing in equation (A5) depend on the original concentration parameter (see M85, Appendix A). For this reason, the filled symbols in Figure 1 are only plotted up to the initial concentration parameter $x_t = 100$. Note also that the absence of filled triangles in Figures 1*a* and 1*c* reflects the fact that the potential at the edge of a halo galaxy is so strong (relative to the potential at the edge of a modified Hubble galaxy of equal central density and core radius) that the tides produced in "parabolic" orbits are too weak to bring the outermost shell to positive energy. The positions of the symbols relative to the dash-dot line in the lower plots of Figure 1 indicate the validity of a Taylor expansion of the tidal field in equation (9): Figure 1*c* shows that the tidal radii derived with both instantaneous and impulsive methods are larger than the distance of the galaxy to the cluster center, thus justifying the method of solving equation (9) exactly. Similarly, Figure 1*d* indicates that $r_t/R \gtrsim 0.3$ for modified Hubble galaxies.

Of course, the impulse approximation may not be valid, since in reality the orbit is not a straight line and the velocity is not constant, or perhaps large enough. However, the trajectories are nearly linear at closest approach for orbits penetrating inside the core radius of the background, because the potential inside the core radius of the modified Hubble model adopted for the background (§ II*c*) is close to that of a harmonic oscillator, producing elliptical orbits centered on the background. And for small departures from linear orbits, Knobloch (1976) has shown that the velocity increments are within a few percent of those derived with the assumption of linear orbits.

Spitzer (1958) and Knobloch (1976) show that the impulse approximation becomes invalid when $V \leq p\omega_g(r_t)$, which translates with equation (11) to $F \geq F_{\text{crit}} = 0.41 p\omega_p(0)/V$. In Figure 2, F_{crit} is plotted as a function of impact parameter for equilibrium orbits, along with the Taylor expansion solutions for F, for reference. By comparing this plot with Figure 1, one sees that for circular equilibrium orbits the impulse approximation is not valid for impact parameters inside the core radius of the perturber, while for "parabolic" orbits the impulse approximation is essentially valid everywhere.

With these constraints in mind, the adopted limiting radius of a galaxy has been chosen as $r_{\text{lim}} = \max(r_{\text{ia}}, r_{\text{ct}})$, where r_{ia} is the limiting radius obtained from the impulse approximation (the filled symbols in Fig. 1) and r_{ct} is the tidal radius obtained from equation (9) for circular orbits (the open circles in Fig. 1). In order to assess the effects of possible inaccuracies in this mean-field limitation scheme, a few simulations are carried out either with no mean-field limitation or with a "modified" tidal radius, chosen as $r_{\text{mt}} = \max(r_{\text{et}}, r_{\text{ct}})$, where r_{et} is the exact tidal radius, the solution of equation (9). For simulations using the modified tidal scheme, mean-field limitation is checked at every time step, rather than right after pericentric approaches.

c) Collisional Stripping

Numerical simulations of fast "hyperbolic" collisions of galaxies have produced a wide range of mass losses: while many authors find that $\Delta M/M$ is usually very low, Dekel, Lecar, and Shaham (1980, hereafter DLS) obtain mass losses reaching 38% for their galaxies of type A (elongated orbits in the envelope). However, Gerhard (1981) points out that the large amounts of mass seen by DLS to escape the test galaxy are probably exchanged between the two galaxies rather than escaping the colliding pair, and suggests that the true mass loss is roughly 4 times smaller than the fraction of mass that escapes one galaxy.

DLS find that the mass loss and the energy change scale as

$$\frac{\Delta M}{M} = \frac{\Delta E}{E} = n v_{\text{col}} , \tag{12a}$$

$$v_{\text{col}} = \frac{(\Delta v)_{\text{rms}}}{v_{\text{rms}}} = \left(\frac{8}{9}\right)^{1/2} \frac{G M_p}{p^2 v} \frac{r_{\text{rms}}}{v_g} , \tag{12b}$$

with $\eta = -\frac{1}{6}$. Here, v_{rms} is a *three-dimensional* velocity dispersion, M_p is the mass of the perturbing galaxy, and r_{rms} and v_g are the root mean square radius and the *one-dimensional* velocity dispersion of the test galaxy, respectively (see Richstone and Malumuth 1983). Note that Aguilar and White (1985) find that $\Delta M/M$ and $\Delta E/E$ are functions of two parameters (perturber mass over velocity at closest approach and impact parameter) instead of one (v_{col}), and are very sensitive to the mass distribution of the galaxies.

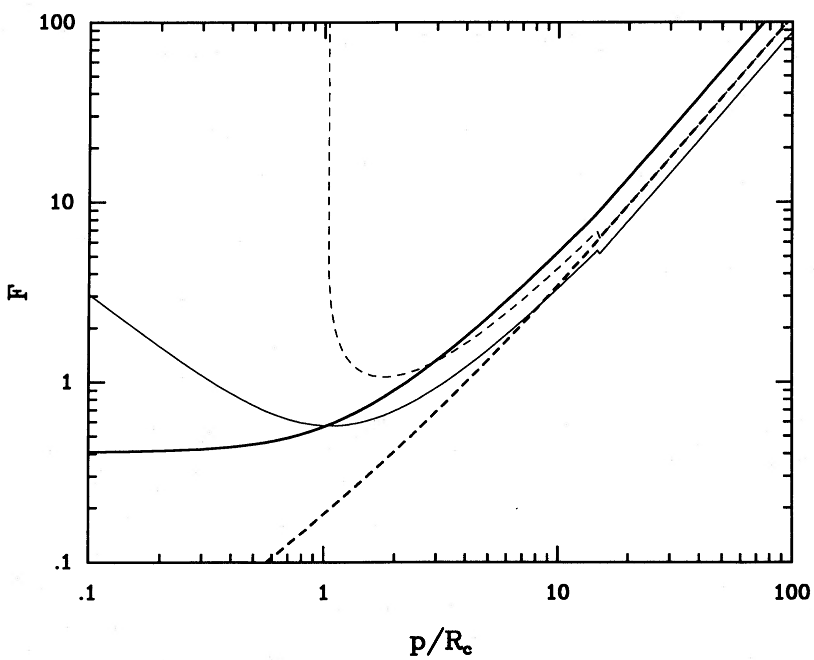

FIG. 2.—Regions of validity of the impulse approximation. *Heavy solid curve*: Critical F for circular galaxian orbits. *Heavy dashed curve*: Critical F for parabolic galaxian orbits. *Thin curves*: Same as the curves in the upper plots of Fig. 1.

Using Merritt's (1981) comparison of Richstone's (1975) tidal efficiencies with those of DLS, and assuming $p_{\max} \approx r_t$ and $p_{\min} \lesssim r_t/3$ (where the mass loss reached its peak efficiency in Richstone's simulations), one then finds that Richstone's mass-loss efficiency satisfies $|\eta| \lesssim 0.042$, i.e., it is at least 4 times lower than that of DLS. Now since, from Gerhard's (1981) argument mentioned above, the mass losses from the latter must have been overestimated by approximately this factor of 4, the present simulations adopt $\eta = -1/24$ along with the parameter dependence of DLS. Note that the other main authors in the field of cluster simulations, Miller (1983), Richstone and Malumuth (1983), and Malumuth and Richstone (1984) have adopted mass losses that are respectively 1.9, 2.7, and 1.6 times those of DLS (M85, § II*c*[ii]), and are thus much too large. Also, DLS noticed that the nearly head-on encounters were much softer than expected from equations (12), so the collisional parameter for close encounters is constrained in the present study by

$$v_{\rm col}(p, v) \leq v_{\rm col}(r_{h_1} + r_{h_2}, v) . \tag{13}$$

It is interesting to compare the results of DLS with the tidal theory exposed in § III*b*. Consider the tides generated by the encounter of a modified Hubble test galaxy of concentration parameter $x_t = 100$ with a modified Hubble perturbing galaxy of the same central density and core radius, with concentration parameter $x_t = 15$. Writing the velocities at closest approach for both circular and "parabolic" orbits in terms of the potential energies of interaction (§ II*a*[i]), the new tidal radius of the test galaxy is found by applying equations (12) and (13) with $\eta = -1/24$, inverting equation (20a), and multiplying by r_c. Figure 3 shows the values of F, obtained from the tidal radius derived above using equation (10), plotted as a function of impact parameter for circular (*circles*) and parabolic (*triangles*) collisions. The results are roughly consistent with the tidal and impulsive results of Figure 1, but the match is far from perfect. This discrepancy could be due to systematic errors in the impulse approximation formulation of the tidal problem given in § III*b*, or this may mean that the simulations of DLS are incomplete, as also suggested by Aguilar and White (1985). Note that the latter authors show that estimates of $\Delta M/M$ and $\Delta E/E$ based on a smooth perturber impulse approximation are close to the corresponding estimates obtained by them from N-body simulations, although they derive the new mass from the velocity increments using a different and more sophisticated method than the one used here in the Appendix.

The deceleration caused by the transfer of orbital energy into the internal degrees of freedom of a galaxy colliding with another one can be calculated if one assumes that the braking occurs before either galaxy sheds mass. In the laboratory frame, this can be written as (M85, § VI*f*)

$$\Delta \boldsymbol{v} = (\boldsymbol{v} - \boldsymbol{v}_p)\left(\frac{M_p}{M + M_p}\right)\left[\left(1 - \frac{\Delta U_t}{T}\right)^{1/2} - 1\right],$$

where $\boldsymbol{v}$ and $\boldsymbol{v}_p$ are the velocities of the test and perturbing galaxy, respectively, M and M_p are their respective masses, T is the bulk kinetic energy of the test galaxy in the center-of-mass frame, and ΔU_t is the change of the internal energy of the test galaxy including the stars escaping from it, and is equal to $2\Delta U$ (DLS, for their type A galaxies).

d) *Mergers*

The numerical experiments of collisions of spherical galaxies by van Albada and van Gorkom (1977), White (1978), and Roos and Norman)1979) have been combined by Aarseth and Fall (1980) to yield the following merger criterion:

$$\left(\frac{v}{1.16 v_{\rm esc}}\right)^2 + \left[\frac{p}{2(r_{h_1} + r_{h_2})}\right]^2 \leq 1 , \tag{14a}$$

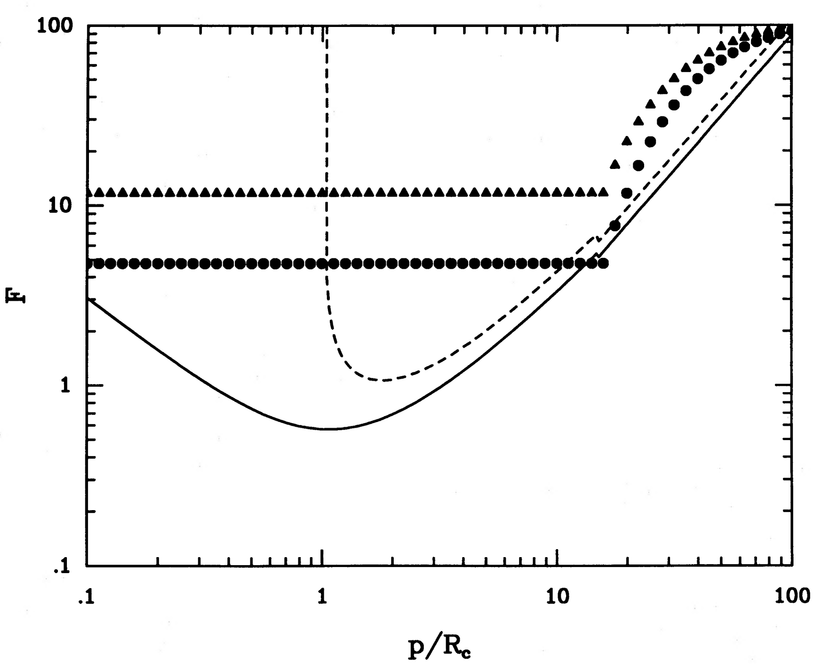

FIG. 3.—Tidal radii transformed to F (eq. [10]) set by collisional stripping using Dekel *et al.*'s (1980) formalism (eqs. [12] and [13]) with $\eta = -1/24$, using modified Hubble test and perturber galaxies with respective concentration parameters $x_t = 100$ and $X_t = 15$, and equal core radii and central densities. *Filled circles*: Circular orbits. *Filled triangles*: "Parabolic" orbits. The solid and dashed curves are the same as in Fig. 1.

where the local escape velocity is defined from

$$\tfrac{1}{2}\mu v_{\rm esc}^2 + V_{\rm int}(p) = 0 , \tag{14b}$$

where μ is the reduced mass of the pair. Farouki and Shapiro (1982) obtain an analogous criterion for mergers of two rotating disk galaxies possessing massive halos, with their spins aligned with the orbital angular momentum:

$$\left(\frac{v}{1.1 v_{\rm esc}}\right)^2 + \left[\frac{p}{5.5(r_{h_1} + r_{h_2})}\right]^2 \leq 1 . \tag{15}$$

This criterion predicts more mergers than the criterion from Aarseth and Fall (1980), which, as pointed out by Farouki and Shapiro (1982), is in part a consequence of the alignment of the galaxy spins with the orbital angular momentum. Collisions of galaxies whose spins are anti-aligned with the orbital angular momentum should yield a merger criterion more similar to that of Aarseth and Fall, while collisions of galaxies with mutually orthogonal angular momentum vectors should lie somewhere in between. The present work mainly uses equations (14), although some runs apply equation (15) instead.

When two galaxies merge into a single entity, a fraction of the stars in both galaxies acquire positive energies and promptly escape from the merging system. Numerical simulations of merging galaxies yield fractional mass losses in the range of 2%–17% (Villumsen 1983, and references therein). The mass loss is quite insensitive to galaxy-type, and in mergers of both ellipticals and disk-halo galaxies these particles carry away a substantial fraction of the angular momentum of the two galaxies (White 1979; Miller and Smith 1980; Gerhard 1981). However, $\Delta M/M$ is sensitive to the collisional parameters (White 1978; Villumsen 1982, 1983). In the present work, it is assumed that, for all mergers, the cannibal does not lose mass, and that one-third of the total mass of the victims escapes into the background, while two-thirds goes to the cannibal. This is equivalent to a total mass loss of 17% for equal-mass mergers, and 7% for a 4-to-1 mass ratio between the cannibal and its victim. Since, in small groups, the typical mass ratio for colliding pairs should be around 4 to 1, this prescription gives mass losses that generally agree with the values given in the literature.

Since one-third of the mass of the victims is assumed to end up in the background rather than in the cannibal, then the cannibal and two-thirds of the matter in its victims should constitute an isolated subsystem during the merging process. The new remnant position and velocity are thus computed by conserving the center-of-mass and the linear momentum of this subsystem. The internal energies of the remnants are computed as follows. At the instant before a cannibal swallows a set of victims (most often just one galaxy), the total energy of the merging system is

$$E_i = U_c + \sum U_v + E_{c,v} , \tag{16}$$

where U_c and U_v are the internal energies of the cannibal and each victim, respectively, while $E_{c,v}$ is the orbital energy of the merging subsystem, defined as

$$E_{c,v} = T_c + \sum T_v + V_1 + V_2 . \tag{17}$$

Here T is the kinetic energy in the center-of-mass frame of the merging system, V_1 is the potential energy binding the victims to the cannibal, and V_2 is the potential energy of the subsystem constituted of the sole victoms. Note that equation (17) is approximate, because in a system of overlapping galaxies the total potential energy of the system is *not* the sum of the internal potential energies of its constituent galaxies and the potential energy of the system of single masses, each representing one galaxy.

Similarly, the total energy of the merging system after the event can be written as

$$E_f = U_r + U_e + E_{r,e} , \tag{18}$$

where U_r and U_e are the internal energies of the remnant and of the system of escaping matter, respectively, while $E_{r,e}$ is the orbital energy of the system constituted by the remnant and the matter escaping to the background, defined in the same fashion as $E_{c,v}$ (eq. [17]). Now the last two terms in equation (18) are both probably small and of opposite signs, and are assumed here to sum to zero. Equating E_i and E_f in equations (16), (17), and (18) with this assumption, the internal energy of the merger remnant is then

$$U_r = U_c + \sum U_v + E_{c,v} . \tag{19}$$

In contrast with the present prescription of equations (17) and (19), Richstone and Malumuth (1983) calculated U_r by conserving the average internal velocity dispersion of the cannibal, though they ran a few simulations in which they neglected the orbital energy $E_{c,v}$. Hausman and Ostriker (1978) chose a more similar remnant internal energy, except that they estimated $E_{c,v}$ by assuming that their cannibal and victim were both point masses in circular orbit, while with the present definition of equation (17) the orbital energy can be positive for nearly head-on encounters (see eqs. [14] and [15]) and is indeed so in roughly one-third of the mergers in the present study. Note that both pairs of authors neglected any escaping matter.

e) Galaxy Evolution

The internal structure of galaxies is subject to change as the galaxies gain internal energy and lose mass, after tidal encounters with other galaxies or with the background. Numerical simulations of colliding galaxies have shown that galaxies, or at least their cores, contract at pericenter approach, then later expand (van Albada and van Gorkom 1977; Miller and Smith 1980). The variations of the internal structure of galaxies have been considered by DLS for nonmerging collisions, and by White (1978) and Farouki, Shapiro, and Duncan (1983) for mergers. Unfortunately, there is no clear-cut picture emerging from these numerical experiments.

The approach taken here is to assume that collisionally stripped galaxies evolve homologously, i.e., at constant concentration parameter. Mergers are also assumed to be homologous (despite the departures from strict homology found in merging galaxies by White 1978 and Farouki, Shapiro, and Duncan 1983). Finally, when they are limited by the background mean field, galaxies are assumed to be sharply truncated and thus retain their core properties.

Expressing the total mass and internal energy in terms of dimensionless variables,

$$M(r) = 4\pi\rho_0 r_c^3 \tilde{M}(x) , \tag{20a}$$

$$U(r) = -4\pi G^2 \rho_0^2 r_c^5 \tilde{U}(x) , \tag{20b}$$

then for homologous evolution, given M, U, and x_t, one can invert equations (20) to obtain

$$r_c = \frac{1}{4} \frac{GM^2}{-U} \frac{\tilde{U}(x_t)}{\tilde{M}^2(x_t)} , \tag{21a}$$

$$r_t = x_t r_c \,, \tag{21b}$$

$$\rho_0 = \frac{16}{\pi G^3} \frac{(-U)^3}{M^5} \frac{\tilde{M}^5(x_t)}{\tilde{U}^3(x_t)} \,. \tag{21c}$$

One can make use of Liouville's theorem to find the new internal energy: conservation of phase-space density imposes $\sigma \sim r_c^{-1}$, and with $U \sim M\sigma^2$ and $r_c \sim M^2/U$ (eq. [21a]), one arrives at $r_c \sim M^{-1}$ and $\kappa = (\Delta M/M)/(\Delta U/U) = \frac{1}{3}$. This agrees with the results of DLS for their collisions of type B (circular stellar orbits) galaxies, and with those of Gerhard (1981). This prescription of conserving phase space density confirms that the galaxies puff up they lose mass.

Alternatively, one can assume that galaxies retain their core properties during collisional stripping, for which case the new concentration parameter is found by solving equation (20a) for x_t; one then easily recovers the internal energy (eq. [20b]) and other parameters, such as the half-mass and rms radii. Note that the constant core evolution usually violates Liouville's theorem.

To derive the luminosities of the galaxies one writes

$$\frac{M}{L} = \frac{\rho_0}{\lambda_0} \frac{\tilde{M}(x_t)}{\tilde{L}(x_t)} \,, \tag{22}$$

where λ_0 is the central luminosity density and where $\tilde{L} = L/(4\pi\lambda_0 r_c^3)$. For homologous evolution, it is simplest to assume that the central mass-to-light ratio is conserved, which from equation (22) translates into constant average M/L during collisional stripping. In mergers, one can assume that the M/L of the matter that escapes from a victim to the background is equal to the average M/L of that victim.

Note that regardless of the type of tidal mechanism, the relative mass loss of a galaxy at a given time step is limited to 25% to avoid spuriously large mass variations arising from extreme conditions.

f) Background Evolution

In the present simulations, the background picks up mass tidally stripped off the galaxies, and acquires energy from this infalling matter and from the dissipation of galactic orbital energy by dynamical friction. For simplicity, the background is assumed to evolve homologously (see § III*d*) as in Schneider and Gunn (1983). One problem with this approach is that falling mass is assumed to settle into equilibrium within the background on a short time scale in comparison with the central dynamical time of the background.

As the galaxies dissipate their orbital energy by dynamical friction, the background heats up. However, as the background absorbs energy at constant mass, it expands in radius. This expansion requires work, since it changes the potential energy of the background with the galaxies. The change in the background internal energy is

$$\Delta U_{\rm bg} = -\Delta U_g - \int_t^{t+\Delta t} \sum_\alpha \boldsymbol{F}_{{\rm df}_\alpha} \cdot \boldsymbol{ds}_\alpha - \int_t^{t+\Delta t} \frac{\partial V_{g-{\rm bg}}}{\partial t}\, dt \,, \tag{23}$$

where U_g is the sum of the galaxian internal energies, the first integral is the work performed by dynamical friction as perceived in the frame of the background, and the second integral is the intrinsic variation of the potential energy of the galaxy-background "binding" (M85, § II*f*). Note that the derivation of equation (23) assumes, as usual, that the internal energy of a galaxy is unaffected by the dynamical friction against the background.

Because the last term in equation (23) is difficult to evaluate numerically, the amount of energy absorbed by the background is evaluated through explicit energy conservation. This reduces mathematically to solving a transcendental equation of the form

$$U_{\rm bg}(R_t) + V_{g-{\rm bg}}(R_t) = E - E_g - T_{\rm bg} \tag{24}$$

for R_t, where the terms on the right-hand side of equation (24) are all known quantities (from left to right: the total energy of the full system, the total energy of the system of galaxies, and the bulk kinetic energy of the background).

The new position and velocity of the background are obtained by conserving the center of mass and the linear momentum of the subsystem constituted by itself and the matter that is being removed from the galaxies. Unfortunately, the internal energy of the background, set through explicit energy conservation, may then occasionally vary by an unreasonable amount. For example, if there is a galaxy near the bottom of the background potential well, then pushing the background to a new position amounts to pulling that galaxy out of the potential well of the background, hence reducing the binding energy of that galaxy to the background and, in compensation, increasing the background internal energy by an abnormal amount. Therefore, if, before recalculating the internal energy of the background, the total energy of the full system is off in absolute value by more than half the old internal energy of the background, then the background is pushed from its old position *with* the galaxy that has the largest binding energy to the background. The energy deficit is recomputed, and if it still does not satisfy the above criterion, the background is pushed from its old position with *two* galaxies instead of one, and so forth. Although, this scheme is somewhat ad hoc, its use is required in less than 1% of the time steps.

IV. INITIALIZATION

a) Positions and Velocities

The initial positions of the galaxies are drawn from a homogeneous distribution inside a sphere of a predetermined radius. The velocities are drawn from a normal distribution with zero mean and unit velocity dispersion, and then normalized, by a constant factor determined by the virial theorem written in its general steady state form (e.g., Goldstein 1950):

$$\sum_\alpha m_\alpha v_\alpha^2 + \sum_\alpha \boldsymbol{F}_\alpha \cdot \boldsymbol{R}_\alpha = 0 \,. \tag{25}$$

Ideally, one would obtain realistic initial condition by allowing the first-order system of particles to relax over a sufficient number of crossing times. However, if one lets a system of particles relax with dynamical friction, the system will contract because of orbital decay, while if one allows the system to relax without dynamical friction, one is then implicitly assuming that dynamical friction abruptly turns on at some point in the history of the group. Therefore, in practice, initial velocities are directly taken from equation (25). Moreover, only the systems in which *all* the galaxies have positive binding energies are considered. For runs with a massive background, rejecting systems with initially unbound galaxies amounts to preferentially selecting systems that are concentrated toward the center and/or that possess a negative velocity dispersion gradient (M85, § V*a*). This thus amounts to the establishment of a library of realistic near-equilibrium initial conditions. Finally, the background is initially centered at the center of mass of the galaxy system, with zero net bulk velocity.

b) *Galaxy Parameters*

In the present simulations, the galaxies are randomly assigned luminosities from a Schechter (1976) distribution of index -1:

$$\Phi(L)dL = (L/L^*)^{-1}e^{-L/L^*}dL\ . \tag{26}$$

This luminosity function is in good agreement with the corresponding ones for the Turner and Gott (1976*a*) groups (Turner and Gott 1976*b*) and for Hickson's (1982) compact groups (Hickson *et al.* 1984), and Turner and Gott (1976*b*) give $L^* = 3.4 \times 10^{10}\ L_{\odot}$, which corresponds to $M_B = -20.85$ (using $M_{B\odot} = 5.48$).[1]

The initial luminosities are obtained using equation (26) with a faint-end cutoff at $L_{\rm min} = x_1 L^*$, where $x_1 = 0.01$. They are further constrained to give an average galaxy luminosity *in each group* that is within 1% of a chosen value (thus imposing roughly the same total mass for each group). For the modified Hubble models in the present numerical models, M/L_B is constant throughout the galaxies with a value of 10, in concordance with the published results for ellipticals (Binney and Mamon 1982; Mamon 1983; Bacon, Monnet, and Simien 1985). For the halo models, the central blue mass-to-luminosity ratio is set to 2, which for $x_t = 100$ (see below) scales to an average M/L_B of 9.4 within the sphere containing half the light, and an average M/L_B of 45.8 for the whole galaxy.

The velocity dispersions of the galaxies are obtained by the Faber-Jackson (1976) relation:

$$\bar{\sigma} = 190\left(\frac{L}{L_{21}}\right)^{1/4}\ \text{km s}^{-1}\ , \tag{27}$$

where L_{21} is the luminosity of a galaxy with $M_B = -21$, i.e., $L_{21} = 3.9 \times 10^{10}\ L_{\odot}$. The constant in equation (27) is taken to be 78% of the value given in Faber and Jackson (1976) in order to account for the difference between measured central velocity dispersion and average galaxy velocity dispersion (M85, § V*b*). Note that equation (27) is used for both modified Hubble and halo galaxy models, even though it is strictly justified only for the former.

Assuming pressure equilibrium, the internal energies of the galaxies are derived from $U = -(3/2)M\bar{\sigma}^2$. Given the mass and internal energy of a galaxy, its central density and core radius are obtained from equations (21), using $x_t = 100$ initially, which conforms to the concentration parameters that Kormendy (1977) tabulated for bright ellipticals by fitting these to King (1966) models. The half-mass radii, tidal radii, and rms radii are then easily derived (see M85, Appendix A).

c) *Background Parameters*

Setting the background "edge" radius to R_t, the internal energy of the background, from equations (21a) and (21b), is

$$U_{\rm bg} = -\frac{1}{4}\,A^2(X_t)\,\frac{GM_{\rm bg}^2}{R_t}\ , \tag{28a}$$

where

$$A(X_t) = \frac{X_t^{1/2}\tilde{U}^{1/2}(X_t)}{\tilde{M}(X_t)}\ . \tag{28b}$$

The core radius and central density of the background can be derived from equations (21b) and (21c), respectively. Finally, the background luminosity is set to zero at the start of each run.

The variation of the internal velocity dispersion of the background as a function of radius (needed to estimate the dynamical friction force) is obtained by solving the isotropic hydrodynamic equation considering the potential terms from the galaxies as well as from the background. If the background is spherically symmetric and if the galaxies are distributed in a sphere centered on the center of the background, one can write this as

$$\frac{d(\rho\sigma^2)}{dR} = -\rho(R)\,\frac{GM_{\rm bg}(R)}{\beta(R)R^2}\ , \tag{29}$$

where $\beta(R) = M_{\rm bg}(R)/[M_{\rm bg}(R) + M_g(R)]$ is the fraction of mass in the background inside a sphere of radius R centered on the background. Here, $M_g(R)$ refers to the total mass in galaxies whose centers lie within the distance R of the center of the background. From equation (29) the background internal velocity dispersion can be approximated as $1/\beta(r)$ times the value that the background internal velocity dispersion would take if the background were isolated. Now since $\beta(R)$ and thus $M_g(R)$ need to be recomputed for each integrator internal time step (§ V), the computations are speeded up by approximating $\beta(R)$ assuming that M_g is constant during the time step, and proportional to $M_{\rm bg}(R)$ inside a radius R_g whose value is the maximum of $R + r_t$ for the galaxies in the background. This yields

$$\begin{aligned}\beta(R) &= \beta_0\ , && R < R_g\ ,\\ &= \frac{M_{\rm bg}(R)}{M_{\rm bg}(R) + M_g(R_g)}\ , && R \geq R_g\ ,\end{aligned}$$

where $\beta_0 = M_{\rm bg}(R_g)/[M_{\rm bg}(R_g) + M_g(R_g)]$.

Note that if the background is small in comparison with the galaxy system, then equation (29) does not hold, since a neighboring galaxy will exert a force away from the center of the background. To alleviate this problem, the size of the background is set initially to be that of the system of galaxies (keeping the concentration parameter fixed): $R_t = R_g = \max\,(R_\alpha + r_{t_\alpha})$. The average internal velocity dispersion of the background, which initially satisfies $U_{\rm bg} = -(3/2)\beta_i M_{\rm bg}\sigma_{\rm bg}^2$, where β_i is the initial background mass fraction, can then be expressed, using equations (28), as

$$\sigma_{\rm bg} = \left[\frac{1}{6}\,\frac{GM_g}{(1-\beta_i)R_g}\right]^{1/2} A(X_t)\ .$$

In the present simulations, $\sigma_{\rm bg}$ is 80% of the one-dimensional velocity dispersion of the galaxy system on the average, with a large scatter.

d) *Scaling*

This study focuses on groups of five, eight, and 20 galaxies. The simulations presented here have been studied in two density regimes. *Dense* groups are designed to appear similar to Hickson's (1982) compact groups, while *loose* groups are

[1] A Hubble constant of $H_0 = 50$ km s^{-1} Mpc^{-1} is used throughout this study.

TABLE 1

Initial Parameters for Groups of Eight Galaxies

Parameter	Dense Groups $-\sigma$	Dense Groups Median	Dense Groups $+\sigma$	Loose Groups $-\sigma$	Loose Groups Median	Loose Groups $+\sigma$
R_g (kpc)	117	117	117	936	936	936
R_c (kpc)	11.2	11.8	12.9	62	67	77
R_h (kpc)	49	51	56	271	293	335
R_t (kpc)	167	177	194	936	1009	1155
R_α (kpc)	48	81.5	114	407	658	884
$R_{\rm H}$ (kpc)	75	89	101	586	710	885
μ	22.4	22.7	23.0	26.8	27.3	27.5

similar to the groups in Turner and Gott's (1976*a*) catalog. The dense groups are scaled to a physical density of eight galaxies per sphere of radius $R_g = 117h_{50}^{-1}$ kpc radius, while the loose groups of eight members start in a sphere of radius $R_g = 936h_{50}^{-1}$ kpc, i.e., the loose groups are 512 times less dense. Table 1 lists the properties of simulated groups of eight members constructed in this fashion. For the dense groups of eight, the smallest projected circumscribed circles have radii $R_{\rm H}$ that are similar to those of the compact groups from Hickson's (1982) catalog (M85, § V*d*).

The galaxies in Hickson's groups have a mean luminosity of roughly L^*, while the mean luminosity of galaxies in the CfA groups (Geller and Huchra 1983) is roughly 20% lower. Such large values are caused by a selection effect toward luminous galaxies in magnitude limited catalogs, and by the luminosity selection implicit in Hickson's compactness criterion (see § VI*a*). In the present simulations, the average galaxy luminosity is usually set to L^* (see § IV*b*), though a few other simulations are carried out with smaller mean galaxy luminosities. Table 2 lists the range of galaxy parameters thus obtained with the standard parameters above.

The initial background mass fractions are taken as $\beta_i = 0.1$ and 0.75 for groups of halo and modified Hubble galaxies, respectively. With the galaxy mass-to-light ratios used here (§ IV*b*) this corresponds to $(M/L)_{\rm group} = 51$ and 40, for groups of halo and modified Hubble galaxies, respectively, in accordance with the values observed for small groups (Gott and Turner 1977; Rood and Dickel 1978). Note that if β_i is much smaller than 0.1, then the galaxies will often dissipate enough orbital energy into the background to make it acquire positive internal energy, hence evaporate.

For the dense groups, the initial background core radius and edge radius are $R_c = 10$ kpc and $R_t = 150$ kpc. Its average internal velocity dispersion is 130 and 210 km s^{-1} for runs with halo galaxies and modified Hubble galaxies, respectively. For the loose groups, the two radii are roughly 8 times larger, while $\sigma_{\rm bg}$ is $8^{1/2}$ times larger in accordance with the virial theorem.

V. NUMERICAL INTEGRATION

The particles in this study are advanced with an Adams-type predictor-corrector method, adapted from Gear (1971), which uses a variable order up to a maximum of 12. The integrator works on internal time steps before interpolating the variables to the external time step set by the user. This "brute-force" method is faster than the renowned Aarseth-Ahmed-Cohen schemes (e.g., Aarseth 1985 and references therein) when the number of particles is less than 25 (Aarseth 1985) because it involves less bookkeeping. On a VAX 11/785, with a UNIX FORTRAN 77 compiler, a simulation of duration $t_{\rm Hubble}$ typically requires 2.5 and 8 minutes of CPU time for dense groups of eight halo galaxies and modified Hubble galaxies, respectively; 2 minutes of CPU time for a loose group of eight galaxies; and 25 minutes of CPU time for a group of 20 galaxies. Approximately two-thirds of the computation time is invested in the advancement of the particles.

The numerical code conserves energy to better than 10^{-3} per run. This is not very impressive, since the code is designed to *explicitly* conserve energy (§ III*f*). However, when dynamical friction is turned off, explicit energy conservation can be bypassed (since the background is no longer heated from orbital energy dissipation of the galaxies; see § III*f*), and energy is then conserved again to better than 10^{-3} per run.

Self-starting conditions must be used after time steps during which mass is transferred to the background, and this increases the computation time. The fraction of time steps for which mass is sent to the background is limited to 10%, by turning off collisional stripping and "modified" mean-field limitation (§ II*b*) when the tidally truncated mass is less than 1% and 5% of the total galaxy mass, respectively. Energy is explicitly conserved whenever mass is transferred from the galaxies to the background.

The strong conservation properties of the code are probably established by the relatively short time steps. Particles are advanced with a time step chosen as a constant times the smaller of the minimum crossing time and the minimum dynamical time, where each minimum is among all bound pairs of particles (including the background). The constant of proportionality is chosen such that the time steps are always smaller than $1/4\pi$ times the shortest circular orbital time for all pairs of particles (see M85, § VII*a*).

The numerical code has also been tested by experimenting with the decay of the circular orbit of a single galaxy around the background. Using a galaxy whose mass is small in comparison with that of the background, fixing ln Λ, and turning

TABLE 2

Initial Galaxy Parameters

Parameter	Halo Galaxies $-\sigma$	Halo Galaxies Median	Halo Galaxies $+\sigma$	Modified Hubble Galaxies $-\sigma$	Modified Hubble Galaxies Median	Modified Hubble Galaxies $+\sigma$
r_c (kpc)	0.37	0.55	0.86	0.34	0.50	0.78
r_h (kpc)	19	28	44	3.9	5.8	9.1
r_t (kpc)	37	55	86	34	50	78
L (10^{11} $L_\odot$)	0.12	0.26	0.64	0.12	0.26	0.64
M (10^{11} $M_\odot$)	5.5	12	29	1.2	2.6	6.4
$\bar{\sigma}$ (km s^{-1})	142	172	216	142	172	216

off mean-field limitation, one obtains a run of R versus t which matches well the theoretical prediction (M85, § VII*b*).

VI. RESULTS

a) Stability and Compactness

Hickson (1982) defines a compact group to meet the following three criteria: it has at least four members, all within 3 mag of the brightest one (membership). The mean surface magnitude on the red POSS (E) plates is smaller than $\mu_{\rm lim}$, where the mean is taken within the smallest circle containing the geometric centers of the members of the group (compactness). No other galaxies in the above magnitude range or brighter lie within a concentric circle of 3 times this radius (isolation).

In the present study, a projected group satisfying these three criteria with Hickson's choice of $\mu_{\rm lim} = 26$ will be called *compact*. The mean group surface magnitude is obtained from the mean group surface brightness in the B band, assuming $B-E = 1.9$ for modified Hubble galaxies (i.e., ellipticals) and $B-E = 1.5$ for halo galaxies (i.e., spirals) conforming to Hickson's (1982) color transformations.

At a given time, a group is viewed along three orthogonal axes. Calling j_s the number of these views for which the group satisfies Hickson's membership and compactness criteria, with

$$\mu_{\rm lim} = 26 + 5 \log_{10}\left(\frac{R_g}{100 \text{ kpc}}\right) - 2.5 \log_{10}\left(\frac{L_{\rm tot}}{5L^*}\right),$$

where R_g and $L_{\rm tot}$ are the respective *initial* size and total luminosity of the group, then the *instability time* of a group will be defined as the time taken for j_s to fall below 1.5. With this definition, instability will occur if merging depletes the number of galaxies (membership) or if evaporation leads to a significantly enlarged group (compactness). Note that for a standard dense group of eight galaxies (§ IV*d*), $\mu_{\rm lim} = 25.83$ in the above definition of stability, so that the instability time for dense groups of eight members is roughly equal to the time taken for a projected group to lose its compact group appearance in Hickson's (1982) sense.

The first result of this study is that *all standard simulations of dense groups produce unstable groups after a Hubble time.* Figure 4 plots the median (*filled circles and thick solid lines*), 16th and 84th percentiles (*crosses and thin solid lines*), and the extreme values (*points and dashed lines*) of j_s versus time for the sets of 50 simulations of initially eight galaxies. Notice how rapidly the groups of galaxies with massive halos become unstable, compared with those without halos. *On the average, the dense groups of halo galaxies are unstable at* 0.75 Gyr, *while the dense groups of modified Hubble galaxies are unstable at* 2.75 Gyr. This is a result of the larger merger cross sections of the halo galaxies, as will be discussed below.

Figure 5 plots for the dense groups the radial coordinates of galaxies in the center-of-mass frame against time. These figures show a hierarchy of orbits: the low-mass galaxies settle on marginally bound elongated orbits, while the heavy ones spiral in toward the center of the background. In the group of halo galaxies (Fig. 5*a*), four galaxies rapidly succumb to mergers within 300 Myr, the first-ranked galaxy decays into the background core, and, although the remaining galaxies do not decay, they cannot escape the large cross section of the first-ranked member, and eventually merge into it. In the group of modified Hubble galaxies (Fig. 5*b*) there is some merging at first, but less than in the previous group. The first-ranked galaxy decays more rapidly than its halo counterparts of Figure 5*a*, while all the other galaxies decay more or less rapidly into the background.

Figure 6 plots the time evolution of j_s for dense groups of five and 20 galaxies. Simulations of dense groups of five galaxies initially yield shorter median instability times (250 Myr and 1.5 Gyr for groups of halo and modified Hubble galaxies, respectively), which are a consequence of needing only two mergers to fail the membership criterion. Note that a group can show two isolated subgroups along a single projection axis, which explains why some groups of 20 galaxies have $j_s > 3$. Starting with 20 galaxies enables the dense groups to survive longer—up to 1.5 and 7.5 Gyr, on the average, for groups of halo and modified Hubble galaxies, respectively. Furthermore, groups of 20 are well enough populated that they witness a separate core/halo evolution as the galaxies attempt to reach energy equipartition. The resulting mass segregation goes far enough for the core to appear compact and isolated, and this is seen in the simulated groups when j_s is defined *without* the restriction of having at least four galaxies within 3 mag of the brightest one (Hickson's membership criterion) and with $\mu_{\rm lim} = 24.5$, as shown in Figure 7. However, these

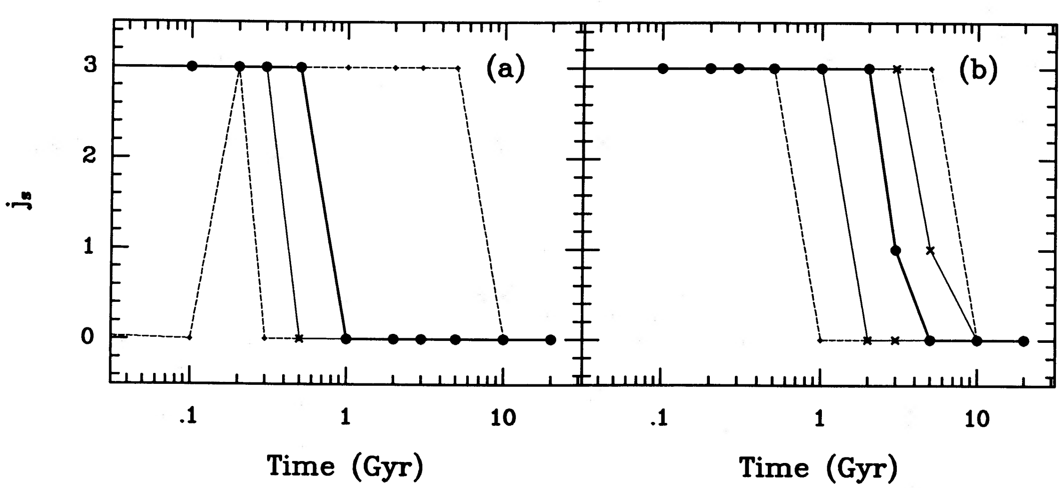

FIG. 4.—Time evolution of j_s in dense groups of (*a*) eight halo and (*b*) eight modified Hubble galaxies. *Filled circles and solid lines*: Median values of j_s. *Crosses and thin lines*: 16th and 84th percentiles. *Points and dashed lines*: Extreme values. The lines are linear interpolations plotted for clarity.

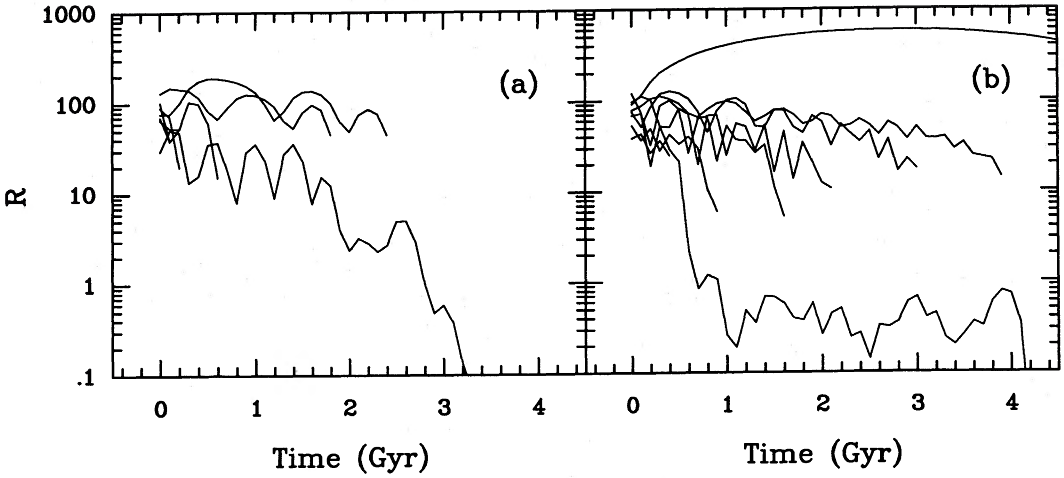

FIG. 5.—Time evolution of galaxy positions with respect to the background, for a dense group of (*a*) eight halo and (*b*) eight modified Hubble galaxies

cores are so dynamically evolved that their brightest members are more than 3 mag brighter than their second-ranked member, thus preventing them from passing the compact-group membership criterion.

In Figure 8, the cumulative number of mergers per run, n_m, is plotted against time for the standard sets of simulations of dense groups of eight and 20 galaxies. The median merger *rate* remains roughly constant after the occurrence of the first merger, until it saturates from the lack of galaxies available for cannibalism (this can be seen better by plotting time on a linear scale). This initial constant merger rate may indicate a balance between the increased cross section of the cannibal and the decreased space density of future victims. The strong inverse correlation of n_m with j_s, easily seen when comparing Figures 4 and 8, suggests that *in dense groups of galaxies, merging is the dominant source of instability*. For a given initial number of galaxies, the merger rates inferred from Figure 8 are higher for groups of halo galaxies than for groups of modified Hubble galaxies. This is caused by the larger half-mass radii of halo galaxies (eq. [14*a*] and Table 2).

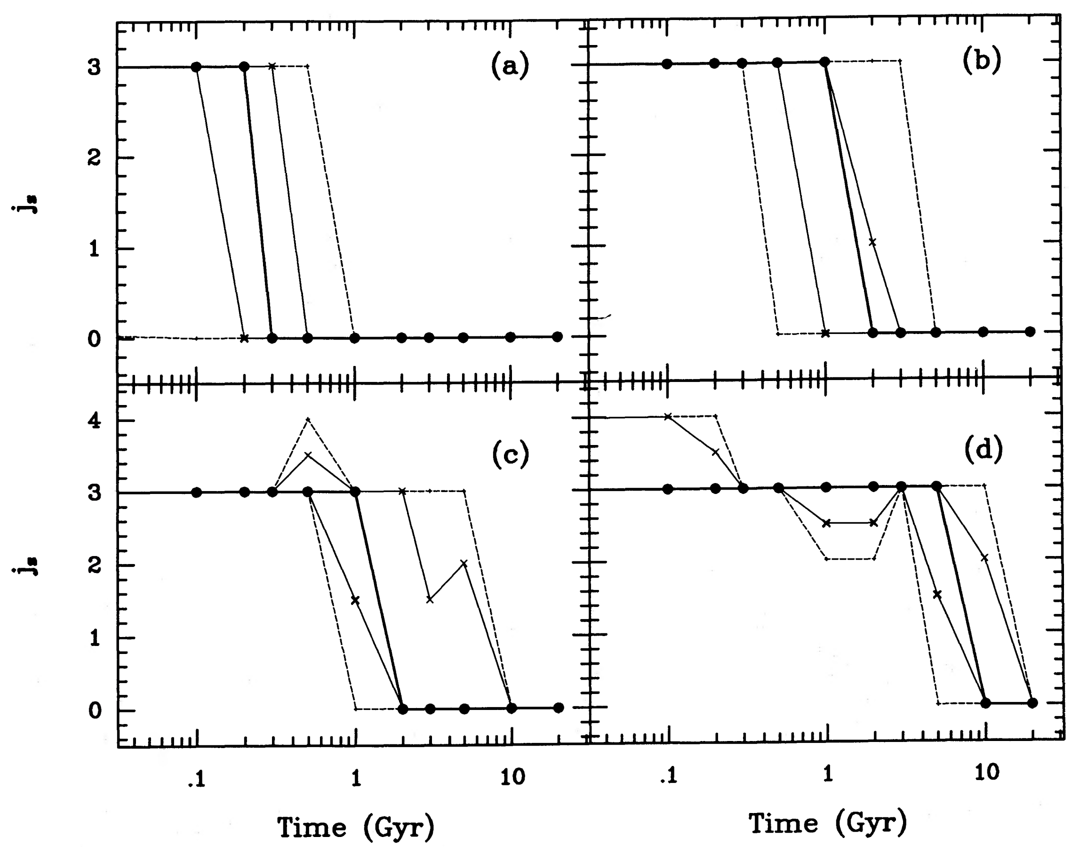

FIG. 6.—Time evolution of j_s for dense groups of five (*a*, *b*) and 20 (*c*, *d*), halo (*a*, *c*) and modified Hubble (*b*, *d*) galaxies. Same notation as in Fig. 4.

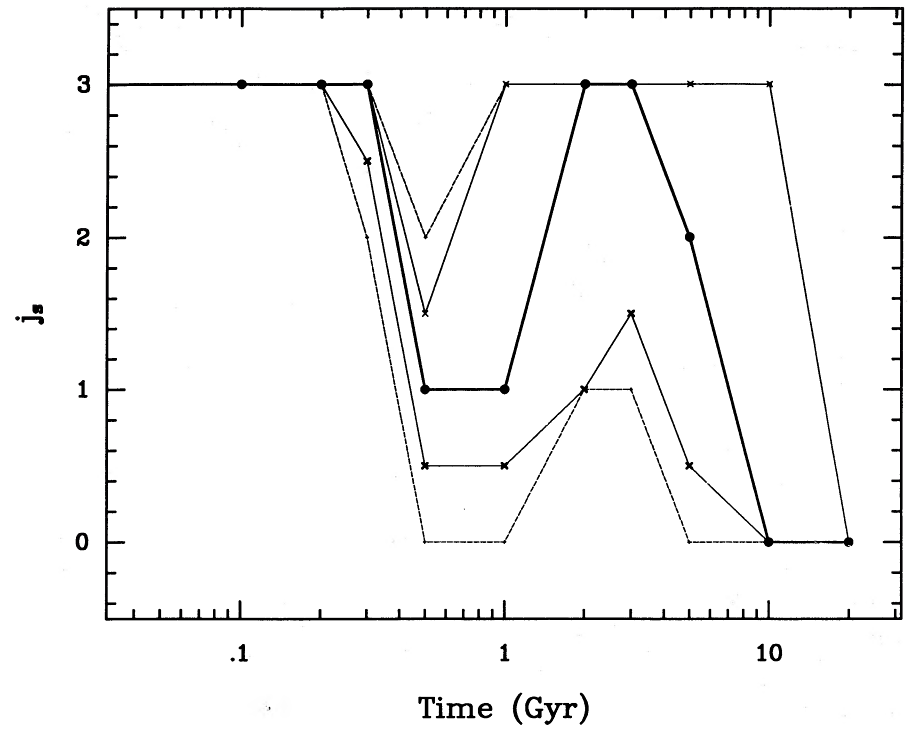

FIG. 7.—Effect of using different criteria in defining stable groups on the time evolution of j_s for dense groups of 20 galaxies. The membership criterion no longer forces the galaxies to lie within 3 mag of the brightest one, and $\mu_{\rm lim} = 24.5$. Same notation as in Fig. 4.

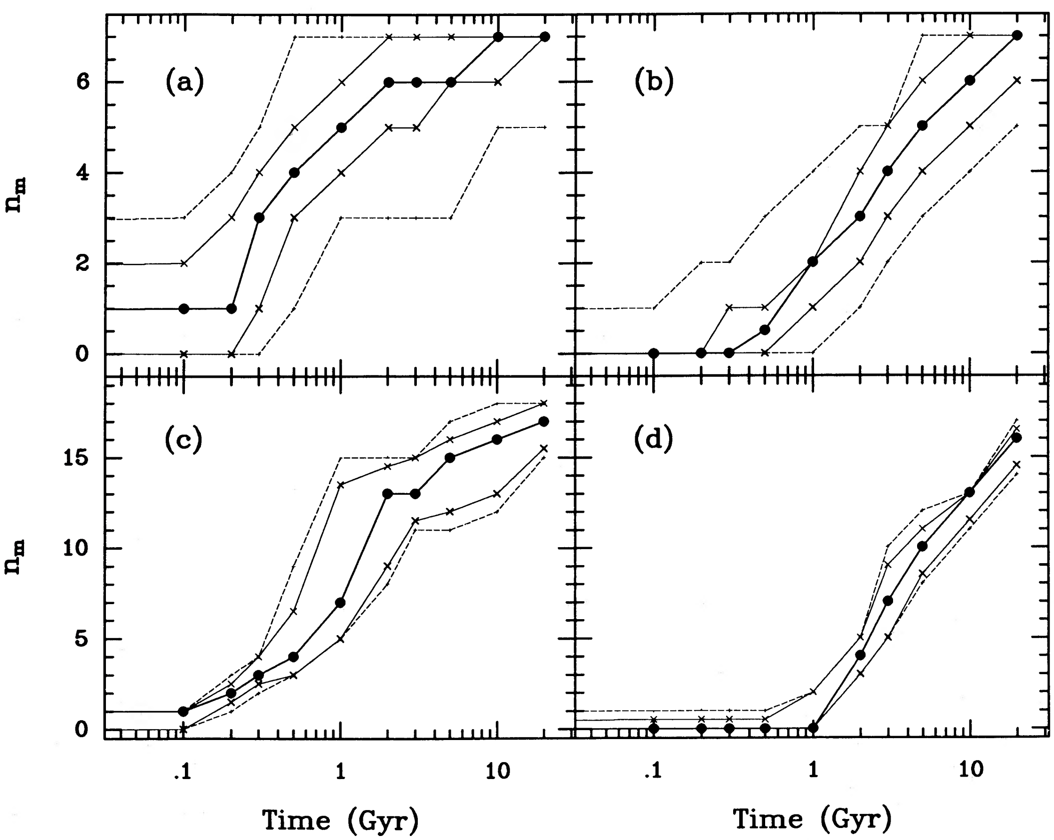

FIG. 8.—Time evolution of the cumulative number of mergers n_m in dense groups of eight (*a*, *b*) and 20 (*c*, *d*), halo (*a*, *c*) and modified Hubble (*b*, *d*) galaxies. Same notation as in Fig. 4.

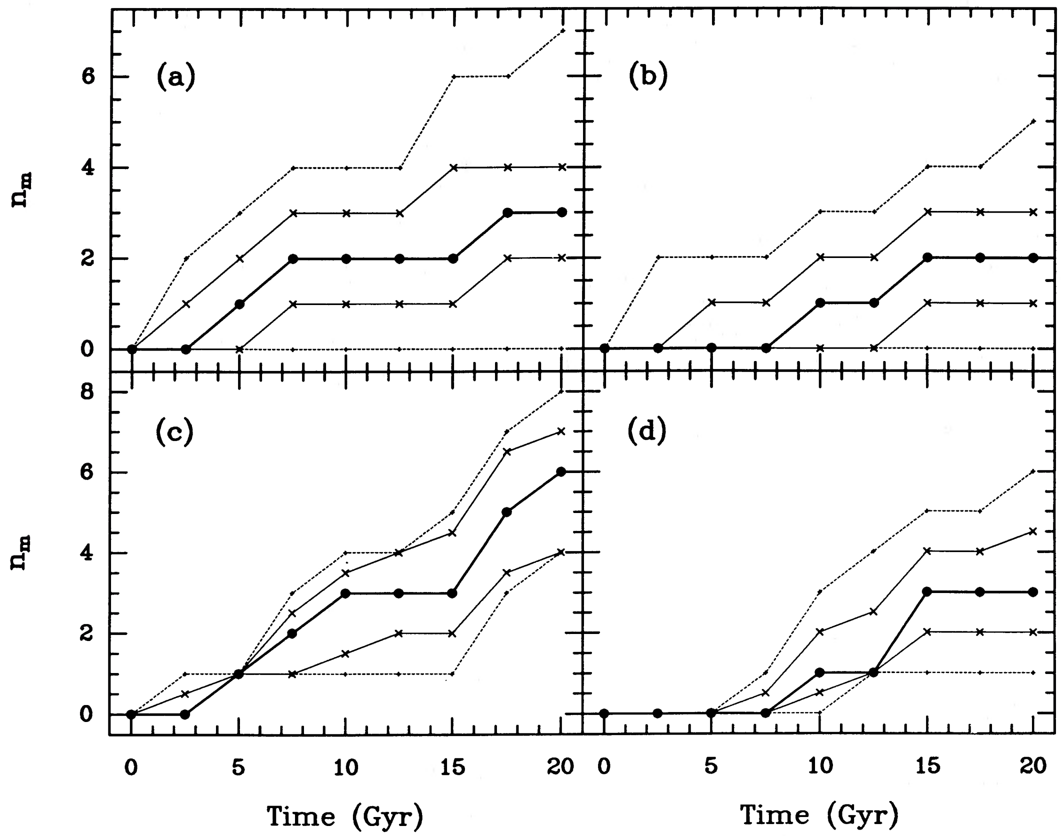

FIG. 9.—Time evolution of the cumulative number of mergers n_m in loose groups of eight and 20 galaxies. Same notation and layout as in Fig. 8.

In Figure 9 the cumulative number of mergers is plotted as a function of time for the standard loose groups. Here the galaxies are more immune to merging, thus enabling most of the loose groups to survive over the Hubble time. Still, 36% and 22% of the respective groups of halo and modified Hubble galaxies have $j_s < 3$ at $t = 20$ Gyr. These two numbers become 55% and 25% when the larger merger cross sections of Farouki and Shapiro (1982) are used. Merger cross sections thus affect more the evolution of groups of halo galaxies than that of their modified Hubble counterparts. Note that loose groups of five galaxies usually lose their stability within $t_{\rm Hubble}$, even with the standard merger cross sections.

The instability times of the dense groups are relatively insensitive to the uncertainties in the physics that is put in the code. For example, if dynamical friction of galaxies against the background is assumed to occur at constant ln Λ, the instability times are decreased by one-third. The effect of uncertainties in the tidal stresses on the galaxies is more important: if background mean-field limitation is assumed to occur at the modified tidal radius, then the instability times are doubled. On the other hand, if mean-field limitation is turned off, the instability times remain roughly the same. If the collisional stripping cross sections are increased fourfold, to the values of Dekel, Lecar, and Shaham (1980), then the instability times are essentially unchanged. Simulations with a background initially stretched out to have twice its usual core radius (and "edge" radius), but with the same mass inside the sphere of radius R_g (containing all the galaxies), produce a similar evolution for the small groups, thus strengthening the validity of the impulsive mean-field limitation scheme described in the Appendix. A more stringent merger criterion (eq. [15]) changes little the instability times of dense groups of modified Hubble galaxies, but reduces the instability times for dense groups of halo galaxies by one-third. The effects of galaxy evolution on the instability times are also small: neither setting κ to 1 (producing galaxy evolution at constant velocity dispersion; see § III*e*) nor assuming constant core evolution instead of homology has any effect on the instability time.

The loose groups are even less influenced by the uncertainties of the input physics. The major change comes with the use of the larger Farouki and Shapiro (1982) merger cross sections, which reduces the instability time of loose groups of eight halo galaxies to $\sim t_{\rm Hubble}$.

The group instability times are more sensitive to the parameters used in the simulations. As long as the total initial group mass is the same, the instability times suffer little change as the initial luminosity function is varied from various Schechter functions to a δ-function. But if the initial background mass fraction is increased to give $(M/L)_{\rm group} = 100$ (instead of 51 and 40 for respective groups of halo and modified Hubble galaxies; § IV*d*), then the instability time is more than doubled.

As seen in Figures 4 and 6, the group instability time fluctuates from one group to the next (where the groups differ only in their initial positions, velocities, and masses but have the same total mass). Roughly two-thirds of the groups are unstable within a factor of 2 of the median instability time, and no dense groups survive past $\frac{1}{2}t_{\rm Hubble}$, except for dense groups of 20 modified Hubble galaxies, which are nevertheless all unstable within $t_{\rm Hubble}$.

It is instructive to express these time scales in terms of a

TABLE 3

GROUP INSTABILITY TIMES

			HALO		MODIFIED HUBBLE	
R_g	N	REMARKS	t_i	t_i/t_{cr}	t_i	t_i/t_{cr}
100......	5	Standard	0.25	2.1	1.5	17
117......	8	Standard	0.75	6.0	2.75	31
117......	8	δ-IMF	0.75	6.0	2.5	28
117......	8	$x_1 = 0.001$	0.40	3.3	2.5	28
117......	8	$L_{tot} = 2L^*$	1.5	6.0	7	43
117......	8	No mean-field limitation	0.75	6.0	3.5	39
117......	8	"Modified" mean-field limitation	1.4	11.1	4	45
117......	8	Dekel *et al.* cross sections	0.75	6.0	2.75	31
117......	8	FS merger criterion (eq. [15])	0.5	4.0	2.75	31
117......	8	Constant core evolution	0.75	6.0	2.75	31
117......	8	$\kappa = 1$	0.75	6.0	2.75	31
117......	8	No dynamical friction	0.75	6.0	>20	>223
117......	8	Constant ln Λ	0.5	4.0	1.6	18
117......	8	Stretched background	0.5	4.0	2.4	27
117......	8	$(M/L)_{group} = 100$	2.5	36	6.25	118
159......	20	Standard	1.5	11.0	7.5	84
800......	5	Standard	13.75	5.3	12.5	10
936......	8	Standard	>20	>7.3	>20	>13
936......	8	FS merger criterion (eq. [15])	20	7.3	>20	>13
1270......	20	Standard	>20	>6.6	>20	>12

dynamical time scale of the initial group. The half-mass crossing time of the system can be defined as

$$t_{cr} = \left(\frac{2\langle R\rangle^3}{GM}\right)^{1/2},$$

where M is the total group mass and $\langle R\rangle$ is the group half-mass radius, approximated as the mass-weighted average of the half-mass radii of the system of galaxies and the background, respectively: $\langle R\rangle = \beta R_h + (1-\beta)\langle R_\alpha\rangle$. Note that this time scale is roughly $1/2\pi$ times the circular orbital time of a galaxy around the group at half-mass radius. Table 3 gives M, $\langle R\rangle$, t_{cr}, the instability time t_i, and t_{cr}/t_i, for various sets of simulations. *The standard dense groups of eight halo galaxies are stable for 6 half-mass crossing times, and the standard dense groups of eight modified Hubble galaxies are stable for approximately 35 half-mass crossing times.*

Table 4 gives the frequency of compact group occurrence within the simulated loose groups: η_1 is the fraction of projected groups at $t > 10$ Gyr that appear compact, and η_2 is the fraction of these compact projected groups that are also compact when viewed along the other two axes. Roughly 3% of the loose groups of five galaxies and 5%–33% of the larger loose groups contain configurations that appear compact when viewed in projection. Loose groups of modified Hubble galaxies are more likely to produce compact subsystems than loose groups of halo galaxies. It is also easier to form compact groups by starting with larger loose groups. Nearly half of the compact projected groups within loose groups of eight modified Hubble galaxies would appear compact viewed along the two other projection axes. This fraction of three-dimensional cores seems smaller for compact projected groups within loose groups of five and 20 galaxies, although the statistics are poor.

TABLE 4

FREQUENCY OF COMPACT CONFIGURATIONS OCCURRING WITHIN LOOSE GROUPS

N	Galaxy Type	κ	η_1	η_2
5......	Halo	$\frac{1}{3}$	0.035 ± 0.016	0 ± 0.600
5......	Modified Hubble	$\frac{1}{3}$	0.031 ± 0.016	0 ± 0.750
8......	Halo	$\frac{1}{3}$	0.055 ± 0.009	0.176 ± 0.088
8......	Modified Hubble	$\frac{1}{3}$	0.239 ± 0.019	0.457 ± 0.091
8......	Halo	1	0.069 ± 0.011	0.140 ± 0.099
8......	Modified Hubble	1	0.250 ± 0.019	0.436 ± 0.087
20......	Halo	$\frac{1}{3}$	0.153 ± 0.046	0 ± 0.273
20......	Modified Hubble	$\frac{1}{3}$	0.333 ± 0.086	0.200 ± 0.200

The best way to check whether a three-dimensional core is bound (physically dense) or unbound (transient; see Rose 1979) is to look for multiple mergers within short time intervals after the appearance of such cores (note that the code stores the exact merger times but looks for cores only every 2.5 Gyr). The median times for two mergers in dense groups of four halo and modified Hubble galaxies are 0.5 and 3 Gyr, respectively, and the corresponding times for three mergers in dense groups of five galaxies are 0.5 and 5 Gyr. Now, of the 19 different three-dimensional cores appearing inside the loose groups of eight modified Hubble galaxies (before the end of the simulations), only one is followed by mergers within the times quoted above, while two more witness mergers that take slightly longer. In addition, one core witnessed two mergers shortly before sampling, and was followed with another merger a little later. Since mergers may be occurring by chance independently of the existence of the cores, then probably no more than 15% of the three-dimensional cores are bound.

Within the loose groups of eight halo galaxies, none of the four three-dimensional cores witness enough mergers in the time intervals quoted above. If, for better statistics, one considers instead all the occurrences of rapidly succeeding merger events, whether or not in the presence of a sampled three-dimensional core, one finds two occurrences of three mergers in less than 2 Gyr within the 50 loose groups. In comparison, using the observed rate of 152 mergers in $20 \times 50 = 1000$ Gyr, Poisson statistics give an expected probability of 0.034 for two mergers occurring at random within 2 Gyr after a merger event, i.e., five expected occurrences of three mergers in 2 Gyr. Therefore, the multiple mergers observed in the simulations of loose groups of halo galaxies are probably all due to chance. In summary, three-dimensional cores occur rarely within loose groups of halo galaxies, and are probably almost always unbound and transient.

b) *Physical Processes in Group Evolution*

The importance of evaporation can be assessed by simulating a group of particles with the usual softened potential energies of interaction but without any of the physics, i.e., with no background, no collisional stripping, no mergers, and so on. It then turns out that, because of the strongly softened potentials, none of the halo-type galaxies and 3% of the modified Hubble galaxies in dense groups manage to escape within the Hubble time. In other words, *because of the extended nature of galaxies, the evaporation time of dense groups is much longer than the Hubble time*, and very much longer than the relaxation time calculated from the standard point-mass formulae derived by Chandrasekhar (1942; cf. M85, § III).

Several simulations of dense groups were carried out in which dynamical friction was artificially turned off. The resulting evolution for groups of halo galaxies is nearly the same as with dynamical friction. On the other hand, the evolution of groups of modified Hubble galaxies is drastically altered. Nearly all modified Hubble groups remain compact after 20 Gyr, at which time only two mergers have taken place on the average. These results confirm what was seen in Figure 5: *in dense groups of halo galaxies, merging occurs before orbital decay, while in dense groups of modified Hubble galaxies, orbital decay precedes merging.* This explains why the merger criterion affects more the groups of halo galaxies, subject to direct merging, than their modified Hubble counterparts, whose instability times are set by the orbital decay time.

In principle, tidal limitation of galaxies ought to slow down the merging instability by reducing the cross sections of the potential cannibals. However, the instability times listed in Table 3 are insensitive to the tidal physics, except that "modified" mean-field limitation produces longer lived groups. On the other hand, the final values of the tidal radius and the luminosity of the first-ranked galaxy, as well as of the background mass fraction and the central surface magnitude, shown in Table 5 in columns (3), (4), (5), and (6), respectively, often show a strong sensitivity to the tidal physics used for the simulations. The initial median values of r_{t_1} are 100 and 91 kpc for groups of halo and modified Hubble galaxies, respectively, while the initial median L_1 and $\mu_{bg}(0)$ are $8.7 \times 10^{10}\ L_\odot$ and infinity for both types of groups. Recall that, initially, β is 0.1 (halo) and 0.75 (modified Hubble). The first-ranked galaxy sizes are strongly reduced by mean-field limitation, especially for groups of modified Hubble galaxies, for which the background is much more important. This effect on r_t influences in turn (to a lesser degree) the other three parameters. The use of modified mean-field tides affects these parameters even more drastically. Finally, turning of collisional stripping has only small effects on r_{t_1}, L_1, β, and $\mu_{bg}(0)$, even with $\kappa = 1$. This holds for both groups of halo and modified Hubble galaxies. But the use of the 4 times larger collisional stripping cross sections of DLS strongly influences these parameters. Therefore, if the cross sections for mass loss given by DLS are largely overestimated, as assumed in this study, then *in dense groups of galaxies, collisional tides are overshadowed by the tides emanating from the mean field of the intergalactic medium, even when ~90% of the dark matter of the group initially lies in galactic halos.* In loose groups, mean-field limitation turns out to be much less effective, because the background is more tenuous to start with.

If the initial background mass fraction is much larger (giving $M/L = 100h_{50}$ for the group), the dense groups survive longer (Table 3). The stronger tides from the background mean field cause reduced merger cross sections and merger rates in groups of halo galaxies, and reduced galaxy masses and orbital decay rates in groups of modified Hubble galaxies. These trends are also present for both halo and modified Hubble galaxy loose groups. Note that, in groups with little background initially, the rate of orbital decay increases as the background grows in mass but eventually decreases when the continued growth of the background reduces substantially the masses of the stripped galaxies.

Because p_{min} scales as the size of galaxy (§ III*a*[ii]), which increases from collisional stripping (because $\kappa = \frac{1}{3}$; see § III*e*), then fixing the Coulomb logarithm produces larger rates of orbital decay (eqs. [6] and [7]), hence shorter instability times in the groups of modified Hubble galaxies.

c) *Evolution of the Luminosity Distribution*

It is interesting to check how group evolution, especially merging, influences the galaxy luminosity function. For this purpose, groups were evolved starting with fixed initial luminosities equally logarithmically spaced over a range of 16, with the same constraint on the total group luminosity. The luminosity functions, averaged over 20 dense groups with these "fixed" initial luminosities, are shown in Figure 10, for $t \approx t_i/2 = 0.5$ Gyr for dense groups of halo galaxies and 1 Gyr for dense groups of modified Hubble galaxies. One detects the appearance of a new magnitude bin at the bright end of the

TABLE 5

FINAL MEDIAN DENSE GROUP PARAMETERS

Galaxy Type	Remarks	r_{t_1} (kpc)	L_1 ($10^{11}\ L_\odot$)	β	$\mu_{bg}(0)$ (B mag arcsec^{-2})
Halo	Standard	44	1.49	0.79	24.7
Halo	$\kappa = 1$	34	1.34	0.83	24.2
Halo	No collisional stripping	36	1.30	0.84	24.3
Halo	No mean-field tides	135	2.00	0.32	25.7
Halo	DLS cross sections	13	0.68	0.97	22.7
Halo	Modified mean-field tides	45	1.35	0.82	24.7
Modified Hubble	Standard	16	1.16	0.89	23.6
Modified Hubble	$\kappa = 1$	15	1.24	0.88	23.7
Modified Hubble	No collisional stripping	17	1.30	0.88	23.8
Modified Hubble	No mean-field tides	327	1.47	0.86	23.1
Modified Hubble	DLS cross sections	13	0.72	0.93	22.8
Modified Hubble	Modified mean-field tides	11	1.12	0.89	23.6

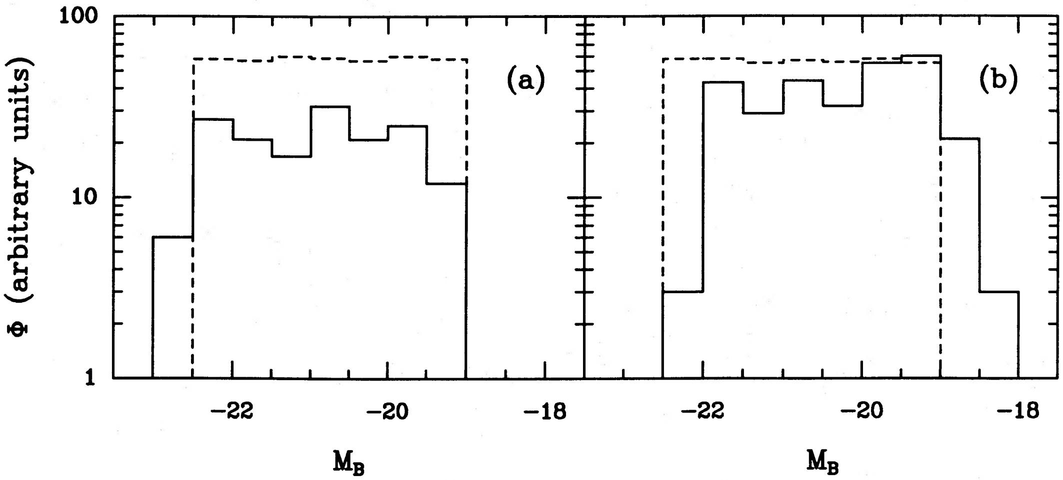

FIG. 10.—Galaxian luminosity functions for compact projected groups within dense groups of (*a*) eight halo and (*b*) eight modified Hubble galaxies, with fixed initial luminosities. *Solid histograms*: Luminosity functions before coalescence (0.5 Gyr) for groups of halo galaxies, and 1 Gyr for groups of modified Hubble galaxies). *Dashed histograms*: Initial luminosity functions.

halo galaxy luminosity function, which houses the better fed cannibals. In comparison, the luminosity function of dense groups of modified Hubble galaxies shows the effects of tidal truncation affecting the brightest galaxies and creating two new bins of fainter galaxies.

The features of the luminosity functions of Figure 10 are not present in the luminosity functions of runs with initial galaxy luminosities sampled from a Schechter function of index −1, cutoff $0.01L^*$ (§ IV*b*), and with the constraint that the average galaxy luminosity *in each group* must be greater than $0.1L^*$. This is seen in Figure 11, which shows the luminosity functions, now averaged over 50 of these runs, at $t = 0$ and $t \approx t_i/2 = 1$ Gyr (halo groups) and 2 Gyr (modified Hubble groups). This occurs because different groups have different first-ranked luminosities, so that the perturbations evident in Figure 10 are washed out in Figure 11. Consequently, *the evolved luminosity functions show little difference from the initial luminosity functions.* The loose groups of galaxies show even less evolution in the luminosity function than their dense counterparts, since, in loose groups, mergers are less frequent and tides are weaker.

Figure 12 shows the evolution of Δm_{12}, the magnitude difference between the first and second brightest galaxies, for compact subgroups of standard dense groups. As expected, Δm_{12} increases rapidly with the cumulative number of merged galaxies. However, this statistic is biased by selecting only subgroups whose brightest and dimmest galaxies are within 3 mag of one another. Nevertheless, the median values of Δm_{12} grow to be quite large ($\gtrsim 1$) before the coalescence of dense groups.

In order to test the significance of the increase in Δm_{12}, one can use the statistic $T_1 = \sigma(m_1)/\langle \Delta m_{12} \rangle$, introduced by Tremaine and Richstone (1977), who show that $T_1 \geq 1$ if the luminosities are randomly sampled from *any* given luminosity function. Hence, T_1 sets upper limits to the mean Δm_{12}, and, if mergers are important in a sample of galaxies, the two inequalities are likely to be violated. However, this statistic is biased by small sample sizes, small set sizes (i.e., group membership), and selection effects (e.g., constraints on the total group luminosity); thus, T_1 is less than unity in most samples of 20 groups of four galaxies with luminosities drawn from the Schechter function (eq. [26]) used to generate Figure 11 (M85, § VIII*c*; Mamon 1987*c*).

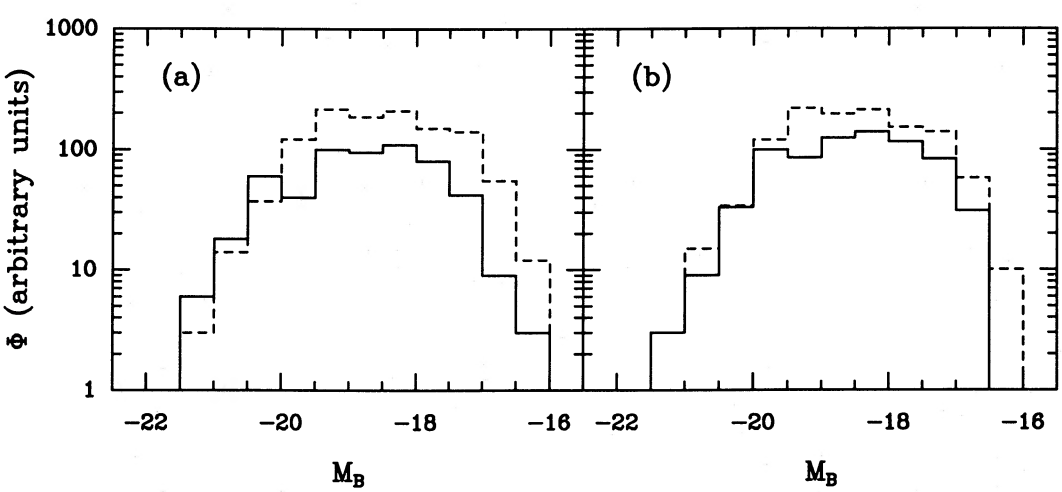

FIG. 11.—Galaxian luminosity functions for compact projected groups within dense groups of eight galaxies, starting with a Schechter luminosity function (without fixing the total group luminosity). Evolved times ar 1 Gyr (halo galaxies) and 2 Gyr (modified Hubble galaxies). Same notation and layout as in Fig. 10.

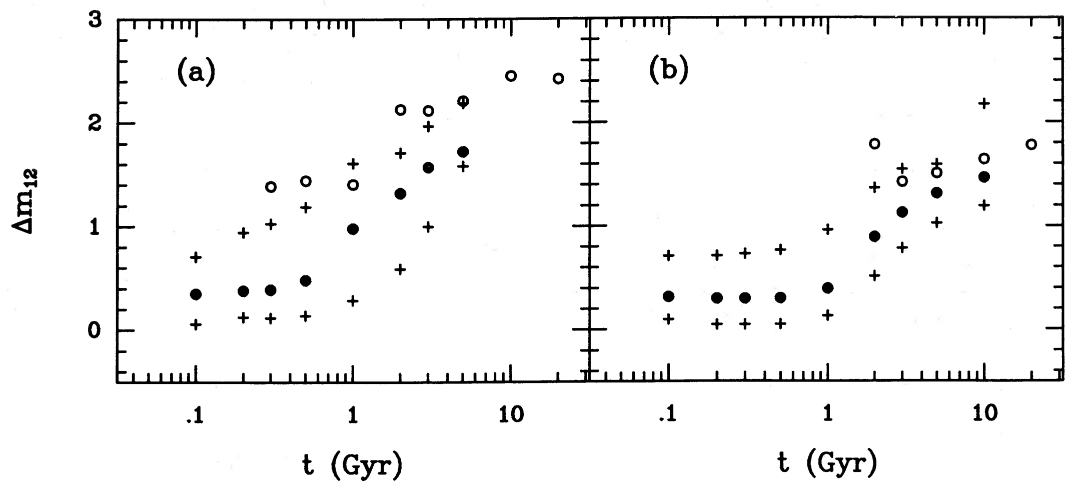

FIG. 12.—Time evolution of Δm_{12} for compact projected groups within dense groups of (*a*) eight halo and (*b*) eight modified Hubble galaxies, with the initial luminosity function of Fig. 11. *Filled circles*: Median values of the compact groups. *Plus signs*: 16th and 84th percentiles ($\pm\sigma$) of the compact groups. *Open circles*: Median values of the noncompact groups.

Despite these limitations, T_1 was generated for the sets of 50 dynamical simulations that started with the luminosity function used to generate Figure 11, and is presented in Table 6 at given group evolution times (for the groups with $j_s > 0$). For comparison, Table 7 shows Monte Carlo estimates of the 5th percentile of T_1, based on 100 trials, obtained using the same luminosity function and with Hickson's (1982) membership criterion (§ VI*a*). One then finds that with 95% confidence the dense groups of eight halo galaxies become incompatible with the Schechter luminosity function used here at 1 Gyr, while their modified Hubble counterparts become incompatible with this luminosity function at 2 Gyr. Another choice of luminosity function would be unlikely to produce the low values of T_1 shown in Table 6. Note that this decreasing trend is also present in Tremaine and Richstone's (1977) T_2 statistic (M85, § VIII*c*). Since the instability times for these runs are 2 Gyr (halo galaxies) and 4.5 Gyr (modified Hubble galaxies), *the bright end of the luminosity functions of evolving dense groups of galaxies show strong inconsistencies with any parent luminosity function roughly halfway through their stable evolution.*

Table 6 also lists the values of T_1 obtained from loose group simulations, starting with a Schechter luminosity function of index -1 and a faint-end cutoff at $0.5L^*$, which gives an average galaxy luminosity of L^* (cf. § IV*d*). Monte Carlo estimates of T_1 with this luminosity function (and again the constraint that at least four galaxies lie within 3 mag from the brightest) yield 5th percentiles of 0.88 for 50 groups of eight galaxies, and 0.80 for 50 groups of four members. Table 6 then indicates that the luminosity functions of loose groups show significant signs of mergers after 7.5 and 10 Gyr for groups of halo and modified Hubble galaxies, respectively. Now, intermediate-density groups ought to have turned around and condensed $10h_{50}^{-1}$ Gyr ago. Therefore, *a large enough catalog of the denser loose groups should show significant evolution in the T_1 statistic.*

Whether or not mergers operate within a small group, the dynamical signature of such a group may be apparent by the amount of luminosity segregation within it. The galaxy luminosity is normalized to the total luminosity in galaxies in the group, and the radial coordinate is taken as the distance of the galaxy to the nonweighted centroid of the group, and normalized to the median distance. Figure 13 plots these quantities for the standard dense groups of halo and modified Hubble galaxies, at $t \approx t_i/2$. While it is difficult to detect by eye in Figure 13 any trend toward luminosity segregation, one can quantitatively estimate the significance of there being no trend with either a linear regression test (e.g., Draper and Smith 1981) or a Spearman rank test (e.g., Press *et al.* 1986).

TABLE 6

T_1 VALUES FOR SIMULATED GROUPS

Time (Gyr)	Dense: Halo	Dense: Modified Hubble	Loose: Halo	Loose: Modified Hubble
0.0	1.12 (50)	1.12 (50)	1.08 (50)	1.08 (50)
0.1	1.10 (50)	1.16 (50)	...	...
0.2	1.02 (50)	1.18 (50)	...	...
0.3	0.93 (49)	1.21 (50)	...	...
0.5	0.80 (48)	1.09 (50)	...	...
1	0.49 (39)	0.92 (50)	...	...
2	0.33 (26)	0.46 (49)	...	...
3.........	0.24 (16)	0.39 (43)	...	...
5	...	0.27 (29)	0.93 (50)	0.96 (50)
7.5	...	...	0.70 (50)	0.86 (50)
10	...	...	0.61 (50)	0.69 (50)
15	...	...	0.46 (48)	0.39 (50)
20	...	...	0.34 (42)	0.24 (49)

NOTE.—Numbers in parentheses refer to the number of runs used in estimating the preceding value of T_1.

TABLE 7

MONTE CARLO ESTIMATES OF T_1 5TH PERCENTILES

$\mathcal{N}$	$N = 8$	$N = 4$
50............	0.99	0.64
40............	0.95	0.60
30............	0.92	0.58
20............	0.79	0.54
15............	0.65	0.53

NOTE.—$\mathcal{N}$ is the number of groups, and N is the number of galaxies in each group.

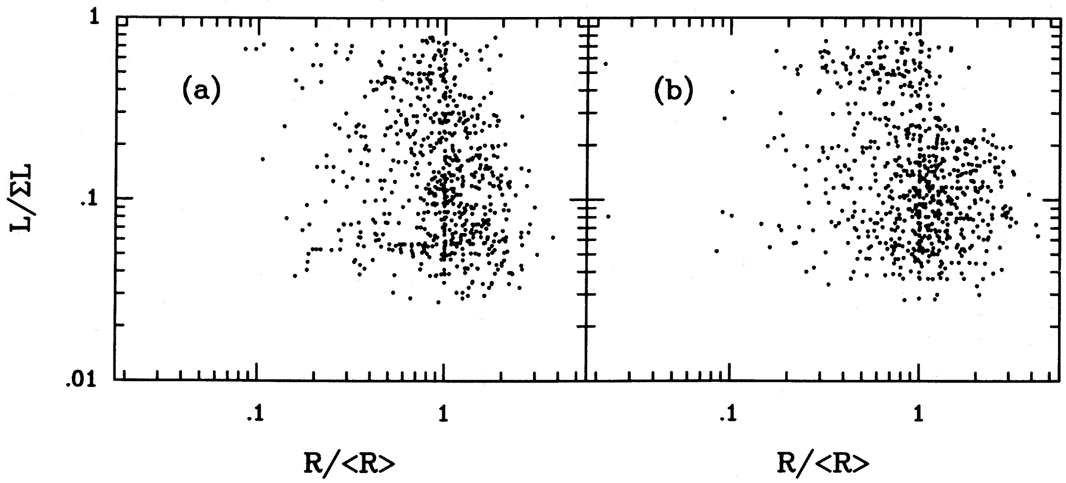

FIG. 13.—Luminosity segregation for dense groups of (*a*) eight halo galaxies at $t = 0.3$ Gyr and (*b*) eight modified Hubble galaxies at $t = 1$ Gyr

The confidence levels for the null hypothesis of no luminosity segregation are shown in Table 8 for simulated groups of eight galaxies. The column heads labeled $P(R)$ and $P(S)$ indicate the values from the regression test and Spearman test, respectively. Dense groups show significant segregation starting at $t = 200$ Myr (halo) and 100 Myr (modified Hubble), while for loose groups the corresponding times are 5 Gyr and 2.5 Gyr. The more rapid luminosity segregation in dense groups of modified Hubble galaxies relative to their halo counterparts may result from differential rates of orbital decay operating in the former groups where the background is more massive. Alternatively, one can use as a radial coordinate the distance of the galaxy to the center of the smallest circumscribed circle, normalized to the radius of this circle, and the results are essentially the same, since segregation occurs after $t = 200$ Myr (dense groups) and $t = 5$ Gyr (loose groups). Unfortunately, this statistic is flawed, because nearly half of the data points lie on the unit abscissa line; furthermore, the center of the circle does not coincide with the center of mass of the group, so that luminosity segregation is washed out in the inner regions of the circle. In any event, *luminosity segregation ought to be detectable in physical groups of galaxies.* Note that the subsample of Hickson's (1982) compact groups with "accordant redshifts" (as defined in Mamon 1986) shows no luminosity segregation, whichever of the two methods described above is used (see also Mamon 1986).

In dense groups, the background expands by roughly a factor of 2 before the onset of coalescence, a consequence of the energy pumped in from dynamical friction on the galaxies. Its central surface magnitude, as seen in Table 5, remains around $\mu_B = 24$, which is about the level of sky in Chile or Hawaii. The background surface brightness averaged within a given aperture is of course smaller. However, one can easily show that for $R_c = 20$ kpc, groups with recession velocities $v < 10{,}000\ (1'/\theta)$ km s^{-1} will have a mean surface magnitude $\mu_B < 25.5$ within a circular aperture of radius θ, which ought to be detectable at the high-altitude sites mentioned above. In loose groups, the background is initially too stretched out ever to be detectable.

d) *Global Group Properties*

Although the virial mass-to-light ratio has large dispersion and systematic biases (Bahcall and Tremaine 1981 and references therein), the median virial mass-to-light ratio of a set of 10 or more groups provides reasonably accurate estimates of the mass interior to these groups (Mamon 1987*a*). The median virial luminosity weighted mass-to-light ratios (as defined in Rood, Rothman, and Turnrose 1970) are shown in Table 9 to decrease significantly in all cases, except for dense groups of

TABLE 8

CONFIDENCE LEVELS FOR ABSENCE OF LUMINOSITY SEGREGATION IN SIMULATED GROUPS

	DENSE GROUPS				LOOSE GROUPS			
	Halo		Modified Hubble		Halo		Modified Hubble	
TIME (Gyr	$P(R)$	$P(S)$	$P(R)$	$P(S)$	$P(R)$	$P(S)$	$P(R)$	$P(S)$
0	× [a]	0.449	0.058	0.025	× [a]	0.473	0.030	0.095
0.1	0.059	0.118	0.011	<0.001	...	...	...	...
0.2	<0.001	<0.001	<0.001	<0.001	...	...	...	...
0.3	<0.001	<0.001	<0.001	<0.001	...	...	...	...
0.5	<0.001	<0.001	<0.001	<0.001	...	...	...	...
1	<0.001	<0.001	<0.001	<0.001	...	...	...	...
2	...	...	<0.001	<0.001	...	...	...	...
3	...	...	<0.001	0.002	...	...	...	...
5	...	...	...	...	0.167	0.039	<0.001	<0.001
10	...	...	...	...	<0.001	<0.001	<0.001	<0.001
20	...	...	...	...	<0.001	<0.001	<0.001	<0.001

[a] The trend is in the opposite sense of luminosity segregation.

TABLE 9

TIME EVOLUTION OF MEDIAN VIRIAL MASS-TO-LIGHT RATIO

TIME (Gyr)	DENSE GROUPS Halo	DENSE GROUPS Modified Hubble	LOOSE GROUPS Halo	LOOSE GROUPS Modified Hubble
0	37.3	70.1	57.0	85.3
0.1	44.3	76.1	...	...
0.2	45.2	63.2	...	...
0.3	44.0	53.6	...	...
0.5	35.3	52.6	...	...
1	46.6	48.3	...	...
2	...	48.9	...	...
3	...	54.0	...	...
5	...	...	55.0	52.5
10	...	...	42.6	37.6
15	...	...	40.0	27.6
20	...	...	36.3	26.9

halo galaxies. This indicates that mass segregation between galaxies and background is occurring from dynamical friction and orbital decay (e.g., Barnes 1984). As the galaxies decay into the background, less background mass lies within the smallest sphere encompassing them. Also, the background expands as the galaxies decay and transfer their orbital energy into it. Finally, some of the matter tidally truncated from the galaxies resettles in the outer regions of the background (because of the assumed homologous background evolution).

Note that the modified Hubble groups start with too much mass in the background. This is a consequence of Limber's bias, since initially the background is more concentrated than the galaxy system (see Smith 1980). Nevertheless, after 2 Gyr, the virial mass-to-light ratios are smaller than 40 for these groups, and this therefore justifies the standard choice of $\beta_i = 0.75$ for them. Simulations with $\beta_i = 0.9$ produced median values of M/L that started around 180 and did not decrease below 110.

As a final point, the sizes of first-ranked galaxies are plotted against the group mean distance between galaxies, assuming here that all the galaxies lie inside the *sphere* of radius R_H (defined in § IV*d*). These plots are shown in Figure 14, for runs with $\kappa = 1$ (so that collisional stripping contributes to *decreased* galaxy sizes), and for groups of eight galaxies at $r \approx t_i/2$ for the dense groups, and $t = t_{\text{Hubble}}$ for the loose groups. Note that the age of the loose groups does not influence their position in this plot. Presumably, the gaps in between the two clouds of points in Figures 14*a* and 14*b* would be filled by groups of intermediate density. Figure 14*b* indicates a trend of decreasing galaxy size with decreasing mean intergalactic distance in groups of modified Hubble galaxies, while there seems to be no such trend in the groups of halo galaxies plotted in Figure 14*a*. These results confirm the fact that the modified Hubble galaxies are more severely truncated than the halo galaxies (§ VI*b*). Note that a similar pair of figures generated from simulations with $\kappa = \frac{1}{3}$ would be very similar to the plots in Figure 14, which indicates that collisional stripping contributes little to the sizes of the first-ranked galaxies in *both* dense and loose groups (cf. § VI*b*).

VII. DISCUSSION

In the early universe, dense groups ought to turn around from their initial Hubble expansion and subsequently virialize in very short times (although one can argue that they would never reach a state of virial equilibrium). The short instability times of $t_{\text{Hubble}}/30$ and $t_{\text{Hubble}}/8$ for dense groups of 8 halo and modified Hubble galaxies, respectively, with $(M/L)_{\text{group}} = 40h_{50}$, make it very difficult to account for present-day compact groups as surviving dense groups formed during the early universe. The spread of the evolution times observed in the present simulations (§ VI*a*) is too small to change this conclusion. Starting with 2.5 times more mass in the groups ($M/L_B = 100h_{50}$), the median instability times become roughly 3 times longer, but are still too short to accommodate an early formation of present-day dense groups. If the mass-to-light ratio of groups were $200h_{50}$ as found by Mezzetti *et al.* (1985) for the groups in the CfA catalog (Geller and Huchra 1983), then the instability times would be even longer. However, these very large mass-to-light ratios probably reflect a significant contamination by interlopers, for otherwise how would Gott and Turner (1977) and Rood and Dickel (1978) find *lower* mass-to-light ratios in small groups? The masses of groups are

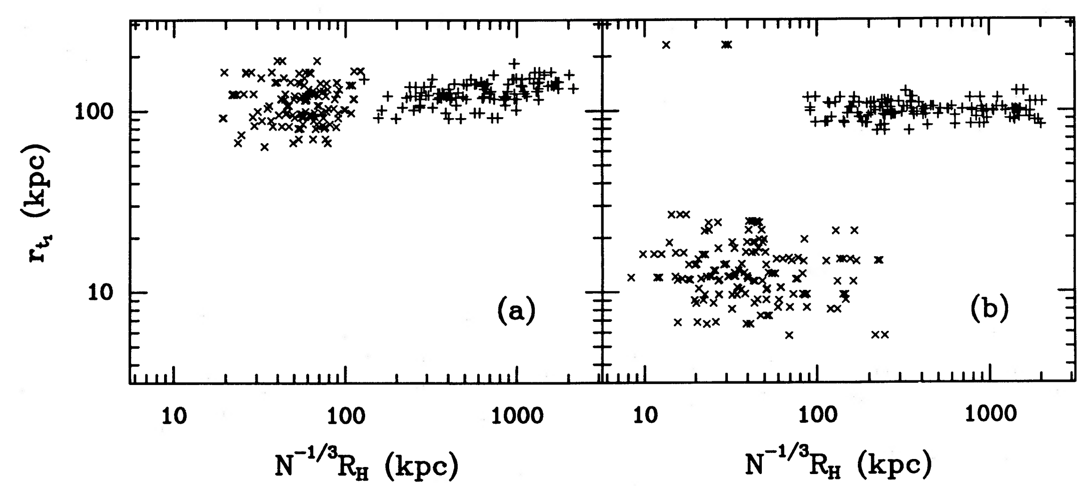

FIG. 14.—Largest galaxy size vs. mean intergalactic separation for groups of eight galaxies with $\kappa = 1$, at $t = 0.3$ Gyr (halo galaxies in dense groups), $t = 1$ Gyr (modified Hubble galaxies in dense groups), and $t = 20$ Gyr (galaxies in loose groups). Same layout as in Fig. 13. *Crosses*: Compact projected groups within dense groups. *Plus signs*: Stable projected groups within loose groups. The gaps between the clouds of points would presumably be filled by points representing intermediate density groups.

hence fundamental in probing the survivability of the densest ones.

Therefore, if a compact group is physically dense and bound today, it must have formed recently via 2-body processes within a loose group. Such an evolution has been observed in the simulations of loose groups presented here, although bound dense subgroups occur rarely ($<1\%$) in loose groups of modified Hubble galaxies and almost never within loose groups of halo galaxies. Note that a bound core within a loose group of modified Hubble galaxies is more likely to be dispersed by encounters with other galaxies from the group than is a corresponding core within a loose group of halo galaxies, because the ratio of instability time to parent group crossing time is much larger in the former case.

With the statistics of projected compact groups seen in simulated loose groups (§ VI*a*), one can reassess the distribution of the states of the compact groups cataloged by Hickson (1982) with "accordant redshifts" (see Mamon 1986). If galaxies in groups possess massive halos, then the vast majority of Hickson's accordant redshift compact groups must be chance alignments within larger loose groups. On the other hand, if galaxies are stripped of their halos at an early stage of the evolution, then roughly 40% of the accordant redshift compact groups must be unbound transient cores, 5% physically dense subgroups, and the remaining 55% chance alignments within loose groups. In any event, the majority of the accordant redshift groups of Hickson's catalog must be chance alignments of galaxies within loose groups, and further arguments for this are presented in Mamon (1986).

In contrast, Rose (1979) simulated loose groups of seven galaxies (with $R_g = 500$ Mpc), and found compact configurations within 12% of his groups, which he attributed to simultaneous transient passages of galaxies through the core of the parent group. The large softening length adopted by Rose (55 kpc) and the absence of intergalactic background in his simulations make his groups directly comparable to the loose groups of halo galaxies here, for which only 15% of the compact projected groups are part of three-dimensional cores. This discrepancy is discussed further in Mamon (1986).

The results from the simulations of small virialized groups of Carnevali, Cavaliere, and Santangelo (1981), Cavaliere *et al.* (1983), and Barnes (1985), although obtained from a very different scheme (by building galaxies with a collection of particles rather than a single one), are nevertheless suitable for comparison with the simulations presented here. The density of the groups in those simulations is inferred from the ratio of the galaxy half-mass radius to the group half-mass radius, and the instability times, inferred from their snapshots, are expressed in units of the group half-mass crossing time. Details of the following analysis are given in M85 (§ IX*b*).

In the present simulations with fixed initial luminosities, the typical ratio of galaxy half-mass radius to group half-mass radius, from the numbers in Tables 1 and 3, are $r_h/\langle R\rangle \approx 0.35$ for dense groups of halo galaxies, 0.1 for dense groups of modified Hubble galaxies, 0.04 for loose groups of halo galaxies, and 0.015 for loose groups of modified Hubble galaxies. In comparison, Carnevali, Cavaliere, and Santangelo (1981) simulated average density groups of 10 or 20 halo-like galaxies, each comprised of 20 stars and no background, and their groups were unstable (in the sense of § VI*a*) in 7 of their time units, corresponding to $t_i \approx 8t_{\rm cr}$. Using the same code, but with a Schechter mass function, Cavaliere *et al.* (1983) arrive at $t_i \approx 7t_{\rm cr}$. With 50% of the group mass in a diffuse background, their instability time extended to $t_i \approx 20t_{\rm cr}$. Finally, model E of Barnes (1985), with five galaxies and $r_h \sim 0.1\langle R\rangle$ and $\beta_i = 0.5$, was unstable in three of his time units, or $t_i \approx 8t_{\rm cr}$, while his group of 10 galaxies (model G) seemed to survive much longer (see his Fig. 5).

To make a direct comparison between model E of Barnes (1985) and the present code, simulations were carried out using five equal-mass modified Hubble galaxies with $r_h = 6.3$ kpc, inside a sphere of radius $R_g = 117$ kpc, and with $\beta_i = 0.5$. As in Barnes, these simulations start with $r_h/\langle R\rangle = 0.1$. The median t_i comes out to be 1.5 Gyr or $t_i/t_{\rm cr} = 7.9$, thus in remarkable agreement with Barnes's result.

In reality, groups do not start out from virialized initial conditions, but instead follow Hubble expansion, then turn around and collapse, and may never pass through a virialized stage. Such initial conditions have been used by Ishizawa *et al.* (1983), Cavaliere *et al.* (1983), and Barnes (1985). A large number of simulations of small groups starting with these more realistic initial conditions, and using the methods presented here, will be presented in a forthcoming paper (Mamon 1987*b*).

This article is largely based upon a Princeton University Ph.D. thesis. The author is indebted to his thesis adviser, Ed Turner, who had suggested a study on compact groups, for his continual advice, as well as to J. P. Ostriker, Luis Aguilar, James Binney, and Paul Hickson for important contributions, and to Cliff Hurvich and Javier Cabrera for statistical advice. Ed Turner and J. P. Ostriker are also thanked for reading the manuscript. Part of the computations were performed on the computers at ADR, thanks to Angel Casado. This work was partially supported by grant AST83-17009 from the National Science Foundation.

APPENDIX

IMPULSE APPROXIMATION FOR A MODIFIED HUBBLE PERTURBER

Consider a stellar system moving past a diffuse distribution of matter. Assume that the trajectory of the diffuse perturber of core radius R_c and central density ρ_s, relative to the stellar system, is a straight line. Let $\boldsymbol{R}$ be the position of the stellar system in the frame of the perturber, and let $\boldsymbol{r}$ be that of a star in the stellar system. The position of the star in the frame of the perturber is then $\boldsymbol{R}_s = \boldsymbol{R} + \boldsymbol{r}$, and the tidal acceleration of a star is

$$\frac{d\boldsymbol{v}}{dt} = \frac{GM(R_s)}{R_s^3}\boldsymbol{R}_s - \frac{GM(R)}{R^3}\boldsymbol{R} = \omega_p^2 R_c\, \boldsymbol{\xi}\,,$$

where $\boldsymbol{\xi}$ is a dimensionless vector and $\omega_p = (4\pi G\rho_0)^{1/2}$. Consider an inertial frame whose first axis points in the direction of the perturber when it is at closest approach, and whose second axis points in the direction of the motion of the perturber. If p is the distance at closest approach, and V is the velocity, assumed constant, of the system relative to the perturber, then using dimensionless variables $\tilde{p} = p/R_c$, $X = R/R_c$, $X_s = R_s/R_c$, $\tilde{x} = x/R_c$, and so on, and writing $X^2 = \tilde{p}^2 + \Omega^2 t^2$ and $X_s^2 = (\tilde{p} - \tilde{x})^2 + (\Omega t - \tilde{y})^2 + \tilde{z}^2$, with $\Omega = V/R_c$, one can write

$$\xi_x = \left[(\tilde{p} + \tilde{x}) \frac{\tilde{M}(X_s)}{X_s^3} - \tilde{p} \frac{\tilde{M}(X)}{X^3}\right],$$

$$\xi_y = \left[(\Omega t + \tilde{y}) \frac{\tilde{M}(X_s)}{X_s^3} - \Omega t \frac{\tilde{M}(X)}{X^3}\right],$$

$$\xi_z = \tilde{z}\left[\frac{\tilde{M}(X_s)}{X_s^3}\right],$$

where $\tilde{M}(x)$ is the dimensionless mass distribution of the perturber (eq. [20a]).

The tidal acceleration can be integrated, yielding

$$\Delta \boldsymbol{v} = \omega_p^2 R_c \int_{-\infty}^{\infty} \xi dt = \frac{2\omega_p^2 R_c}{\Omega} \boldsymbol{\eta}, \tag{A1}$$

with

$$\eta_x = (\tilde{p} + \tilde{x}) I(\tilde{q}) - \tilde{p} I(\tilde{p}), \tag{A2a}$$

$$\eta_y = 0, \tag{A2b}$$

$$\eta_z = \tilde{z} I(\tilde{q}), \tag{A2c}$$

where

$$I(x) = \int_x^{\infty} \frac{\tilde{M}(y) dy}{y^2 (y^2 - x^2)^{1/2}},$$

and $\tilde{q} = [(\tilde{p} + \tilde{x})^2 + \tilde{z}^2]^{1/2}$. For a modified Hubble perturber (eq. [1] with $n = 3$), and with some algebra, one obtains

$$I(x) = \frac{1}{2}\left(\frac{X_t}{X_t^2 + 1}\right)^{1/2}, \qquad x = 0, \tag{A3a}$$

$$\begin{aligned} I(x) = {} & \frac{\sinh^{-1} X_t}{x^2} - \frac{X_t}{x^2 (X_t^2 + 1)^{1/2}} - \frac{\pi}{4x} + \frac{1}{x^2}\left(\frac{X_t^2 - x^2}{X_t^2 + 1}\right)^{1/2} \\ & + \frac{1}{x} \tan^{-1}\left[\frac{1}{x}\left(\frac{X_t^2 - x^2}{X_t^2 + 1}\right)^{1/2}\right] - \frac{1}{2x} \sin^{-1}\left[\frac{X_t^2 (1 - x^2) - 2x^2}{X_t^2 (x^2 + 1)}\right] \\ & + \frac{1}{2x^2} \ln (x^2 + 1) - \frac{1}{x^2} \ln [(X_t^2 + 1)^{1/2} + (X_t^2 - x^2)^{1/2}], \qquad 0 < x < X_t, \end{aligned} \tag{A3b}$$

$$I(x) = \frac{\sinh^{-1} X_t}{x^2} - \frac{X_t}{x^2 (X_t^2 + 1)^{1/2}}, \qquad x \geq X_t, \tag{A3c}$$

where X_t is the concentration parameter of the perturber. Note that if $\tilde{p}$ and $\tilde{q}$ are both greater than X_t everywhere, the velocity changes reduce to those of Spitzer (1958), since the stellar system sees a point-mass potential.

Given $\Delta \boldsymbol{v}$, the limiting radius of the system is defined as the radius of the shell whose new specific energy, relative to the center of the system, is just zero (White 1983). Writing the new specific energy of a star as $E_f = \frac{1}{2}v^2 + \phi(r) + \boldsymbol{v} \cdot \Delta \boldsymbol{v} + \frac{1}{2}(\Delta v)^2$, the specific energy of a shell is obtained by averaging the stellar energies over velocities and then over angles. Assuming velocity isotropy and no rotational streaming, this yields

$$E(r) = \tfrac{3}{2}\sigma^2(r) + \phi(r) + \tfrac{1}{2}\langle(\Delta v)^2\rangle_{\hat{r}}, \tag{A4a}$$

with

$$\langle(\Delta v)^2\rangle_{\hat{r}} = \frac{4\omega_p^4 R_c^2}{\Omega^2} \frac{\iint \eta^2 \sin \theta d\theta d\phi}{4\pi} = \frac{4\omega_p^4 R_c^2}{\Omega^2} \bar{\eta}^2(\tilde{r}, \tilde{p}), \tag{A4b}$$

where η is taken from equations (A2) and (A3). Setting to zero the specific binding energy of the shell, formulated in equations (A4), and expressing quantities in dimensionless form, one arrives at

$$\frac{3}{2} \tilde{\sigma}^2(x_t) - \tilde{\phi}(x_t) + \frac{2\gamma^2 \omega_p^4}{\omega_g^2 \Omega^2} \bar{\eta}^2\left(\frac{x_t}{\gamma}, \tilde{p}\right) = 0, \tag{A5}$$

where r_c and ρ_g are respectively the core radius and the central density of the stellar system, and where $\tilde{\sigma}^2 = \sigma^2/(4\pi G \rho_g r_c^2)$, $\tilde{\phi} = -\phi/(4\pi G \rho_g r_c^2)$, $\gamma = R_c/r_c$, and $\omega_g = (4\pi G \rho_g)^{1/2}$.

If the velocity dispersions are derived with the assumption of isotropy, then the shell binding energy $f_1(x) = \tilde{\phi}(x) - (3/2)\tilde{\sigma}^2(x)$ is a nonmonotonic function of x near the edge of the galaxy (M85, Appendix C). Since $\bar{\eta}^2(x/\gamma, \tilde{p})$ is either monotonic in x, or close to being so (M85, Appendix C), then equation (A5) may have more than one solution, and it is technically difficult to isolate the smallest (i.e., physical) solution when the total number of solutions is not known. Therefore, in practice, the internal velocity dispersion of a galaxy is approximated to the value set by assuming local virial equilibrium, giving an approximate shell binding energy (White 1983) $f_2(x) = \frac{1}{2}\tilde{\phi}(x)$, which is a monotonic function of x. Then the new concentration parameter of the galaxy is obtained by solving

$$\frac{2\gamma^2\omega_p^4}{\omega_g^2\Omega^2}\,\bar{\eta}^2\left(\frac{x_t}{\gamma}, \tilde{p}\right) = \frac{1}{2}\,\tilde{\phi}(x_t) \tag{A6}$$

for x_t, where $\bar{\eta}$ is cubic spline–interpolated from precomputed values.

REFERENCES

Aarseth, S. J. 1985, in *Multiple Time Scales*, ed. J. U. Brackbill and B. I. Cohen (Orlando: Academic), p. 378.
Aarseth, S. J., and Fall, M. 1980, *Ap. J.*, **236**, 43.
Aarseth, S. J., and Saslaw, W. C. 1972, *Ap. J.*, **172**, 17.
Aguilar, L. A., and White, S. D. M. 1985, *Ap. J.*, **295**, 374.
Ambartsumian, V. A. 1961, *A.J.*, **66**, 536.
Bacon, R., Monnet, G., and Simien, F. 1985, *Astr. Ap.*, **152**, 315.
Bahcall, J. N., and Tremaine, S. 1981, *Ap. J.*, **244**, 805.
Bahcall, N. A. 1979, *Ap. J.*, **232**, 689.
Barnes, J. 1984, *M.N.R.A.S.*, **208**, 873.
———. 1985, *M.N.R.A.S.*, **215**, 517.
Binney, J., and Mamon, G. A. 1982, *M.N.R.A.S.*, **200**, 361.
Carnevali, P., Cavaliere, A., and Santangelo, P. 1981, *Ap. J.*, **249**, 449.
Cavaliere, A., Santangelo, P., Tarquini, G., and Vittorio, N. 1982, in *Clustering in the Universe*, ed. D. Gerbal and A. Mazure (Gif-sur-Yvette: Editions Frontières), p. 25.
Chandrasekhar, S. 1942, *Principles of Stellar Dynamics* (Chicago: University of Chicago Press), chap. 2.
———. 1943, *Ap. J.*, **97**, 255.
Cooper, R. G., and Miller, R. H. 1981, *Ap. J.*, **254**, 16.
Dekel, A., Lecar, M., and Shaham, J. 1980, *Ap. J.*, **241**, 946 (DLS).
de Vaucouleurs, G. 1975, in *Stars and Stellar Systems*, Vol. **9**, *Galaxies and the Universe*, ed. A. Sandage, M. Sandage, and J. Kristian (Chicago: University of Chicago Press), p. 557.
Draper, N. R., and Smith, H. 1981, *Applied Regression Analysis* (2d ed.; New York: Wiley), chap. 1.
Faber, S. M., and Jackson, R. 1976, *Ap. J.*, **204**, 668.
Farouki, R., and Shapiro, S. L. 1982, *Ap. J.*, **259**, 103.
Farouki, R., Shapiro, S. L., and Duncan, M. J. 1983, *Ap. J.*, **265**, 597.
Gear, C. W. 1971, *Numerical Initial Value Problems in Ordinary Differential Equations* (Englewood Cliffs, NJ: Prentice-Hall).
Geller, M. J., and Huchra, J. P. 1983, *Ap. J. Suppl.*, **52**, 61.
Gerhard, O. E. 1981, *M.N.R.A.S.*, **197**, 179.
Giuricin, G., Mardirossian, F., Mezzetti, M., and Santangelo, P. 1984, *Ap. J.*, **277**, 38.
Goldstein, H. 1950, *Classical Mechanics* (Reading, MA: Addison-Wesley), chap. 3.
Gott, J. R., and Turner, E. L. 1977, *Ap. J.*, **213**, 309.
Gunn, J. E. 1974, *Comm. Ap.*, **6**, 7.
———. 1977, *Ap. J.*, **218**, 592.
Hausman, M., and Ostriker, J. P. 1978, *Ap. J.*, **224**, 320.
Hickson, P. 1982, *Ap. J.*, **255**, 382.
Hickson, P., Ninkov, Z., Huchra, J. P., and Mamon, G. A. 1984, in *Clusters and Groups of Galaxies*, ed. F. Mardirossian, G. Giuricin, and M. Mezzetti (Dordrecht: Reidel), p. 367.
Ishizawa, T., Matsumoto, R., Tajima, T., Kageyama, H., and Sakai, H. 1983, *Pub. Astr. Soc. Japan*, **35**, 61.
King, I. R. 1962, *A.J.*, **67**, 471.
———. 1966, *Ap. J.* **71**, 64.
Knobloch, E. 1976, *Ap. J.*, **209**, 411.
Kormendy, J. 1977, *Ap. J.*, **218**, 333.
Malumuth, E. M., and Richstone, D. O. 1984, *Ap. J.*, **276**, 413.
Mamon, G. A. 1983, in *IAU Symposium 100, Internal Kinematics and Dynamics of Galaxies*, ed. E. Athanassoula (Dordrecht: Reidel), p. 295.
———. 1985, Ph.D. thesis, Princeton University (M85).
———. 1986, *Ap. J.*, **307**, 426.
———. 1987*a*, in *IAU Symposium 117, Dark Matter in the Universe*, ed. J. Kormendy and G. R. Knapp (Dordrecht: Reidel), p. 114.
———. 1987*b*, in preparation.
———. 1987*c*, in preparation.
Merritt, D. 1981, Ph.D. thesis, Princeton University.
———. 1984, *Ap. J.*, **276**, 26.
Merritt, D., and White, S. D. M. 1987, in *IAU Symposium 117, Dark Matter in the Universe*, ed. J. Kormendy and G. R. Knapp (Dordrecht: Reidel), p. 283.
Mezzetti, M., Pisani, A., Giuricin, G., and Mardirossian, F. 1985, *Astr. Ap.*, **143**, 188.
Miller, G. E. 1983, *Ap. J.*, **268**, 495.
Miller, R. H., and Smith, B. F. 1980, *Ap. J.*, **235**, 421.
Ostriker, J. P., and Hausman, M. 1977, *Ap. J. (Letters)*, **217**, L125.
Ostriker, J. P., Spitzer, L., and Chevalier, R. A. 1972, *Ap. J. (Letters)*, **176**, L51.
Peebles, J. 1970, *A.J.*, **75**, 13.
Press, W. H., Flannery, B. P., Teukolsky, S. A., and Vetterling, W. T. 1986, *Numerical Recipes* (Cambridge: Cambridge University Press), chap. 13.
Richstone, D. O. 1975, *Ap. J.*, **200**, 535.
Richstone, D. O., and Malumuth, E. M. 1983, *Ap. J.*, **268**, 30.
Rood, H. J., and Dickel, J. R. 1978, *Ap. J.*, **224**, 724.
Rood, H. J., Rothman, V. C. A., and Turnrose, B. E. 1970, *Ap. J.*, **162**, 411.
Roos, N. 1981, *Astr. Ap.*, **95**, 349.
Roos, N., and Aarseth, S. J. 1982, *Astr. Ap.*, **114**, 41.
Roos, N., and Norman, C. A. 1979, *Astr. Ap.*, **76**, 75.
Rose, J. A. 1979, *Ap. J.*, **231**, 10.
Schechter, P. 1976, *Ap. J.*, **203**, 297.
Schneider, D., and Gunn, J. E. 1983, *Ap. J.*, **263**, 14.
Smith, H. 1980, *Ap. J.*, **241**, 63.
Spitzer, L. 1958, *Ap. J.*, **127**, 17.
Toomre, A., and Toomre, J. 1972, *Ap. J.*, **178**, 623.
Tremaine, S. D., Ostriker, J. P., and Spitzer, L. 1975, *Ap. J.*, **196**, 407.
Tremaine, S. D., and Richstone, D. O. 1977, *Ap. J.*, **212**, 311.
Turner, E. L., and Gott, J. R. 1976*a*, *Ap. J. Suppl.*, **32**, 409.
———. 1976*b*, *Ap. J.*, **209**, 6.
van Albada, T. S., and van Gorkom, J. H. 1977, *Astr. Ap.*, **54**, 121.
van den Bergh, S. 1962, *Zs. f. Ap.*, **55**, 21.
Villumsen, J. V. 1982, *M.N.R.A.S.*, **199**, 493.
———. 1983, *M.N.R.A.S.*, **204**, 219.
White, S. D. M. 1976, *M.N.R.A.S.*, **174**, 467.
———. 1978, *M.N.R.A.S.*, **184**, 185.
———. 1979, *M.N.R.A.S.*, **189**, 831.
———. 1983, in *Morphology and Dynamics of Galaxies*, ed. L. Martinet and M. Mayor (Sauverny: Geneva Observatory), p. 289.

GARY A. MAMON: Department of Physics, New York University, 4 Washington Place, New York, NY 10003